Search for Quasiparticle Scattering in the Quark-Gluon Plasma with Jet Splittings in *pp* and Pb-Pb Collisions at $\sqrt{s_{\mathrm{NN}}} = 5.02$ TeV

S. Acharya *et al.*[*]
(ALICE Collaboration)

(Received 30 October 2024; revised 27 March 2025; accepted 30 April 2025; published 16 July 2025)

The ALICE Collaboration reports measurements of the large relative transverse momentum (k_T) component of jet substructure in pp and Pb-Pb collisions at center-of-mass energy per nucleon pair $\sqrt{s_{\mathrm{NN}}} = 5.02$ TeV. Enhancement in the yield of such large-k_{T} emissions in head-on Pb-Pb collisions is predicted to arise from partonic scattering with quasiparticles of the quark-gluon plasma. The analysis utilizes charged-particle jets reconstructed by the anti-k_{T} algorithm with resolution parameter $R = 0.2$ in the transverse-momentum interval $60 < p_{\mathrm{T,ch,jet}} < 80$ GeV/c. The soft drop and dynamical grooming algorithms are used to identify high transverse momentum splittings in the jet shower. Comparison of measurements in Pb-Pb and pp collisions shows medium-induced narrowing, corresponding to yield suppression of high-k_T splittings, in contrast to the expectation of yield enhancement due to quasiparticle scattering. The measurements are compared to theoretical model calculations incorporating jet modification due to jet-medium interactions ("jet quenching"), both with and without quasiparticle scattering effects. These measurements provide new insight into the underlying mechanisms and theoretical modeling of jet quenching.

DOI: 10.1103/PhysRevLett.135.031901

Strongly interacting matter at high temperature and density forms a deconfined state known as the quark-gluon plasma (QGP) [1,2]. The QGP filled the universe a few microseconds after the big bang, and it is generated and studied today using high-energy nuclear collisions at the Relativistic Heavy-ion Collider (RHIC) and the Large Hadron Collider (LHC) [3–6]. RHIC and LHC measurements, together with theoretical studies, have revealed that the QGP exhibits marked emergent features; it flows with low specific viscosity and is opaque to the passage of energetic partons [7–9]. While static properties of the QGP can be calculated numerically using quantum chromodynamics (QCD) implemented on the lattice [10,11], the microscopic mechanisms underlying these dynamical phenomena remain poorly understood.

In high-energy hadronic collisions, partons from the projectiles may scatter with high momentum transfer. Such scattered partons are initially highly virtual and evolve by radiating secondary partons that hadronize in a collimated spray of particles which is observable experimentally, denoted a "jet." The jet shower has rich internal substructure that is observable in correlations between its constituent particles. In pp collisions, jet production cross sections and substructure have been measured extensively [12–16]. Theoretical calculations at high perturbative order (pQCD) agree well with the measurements, providing stringent tests of QCD [12,15,17–20]. Charged-particle jets are especially well suited for jet substructure measurement, due to the excellent angular resolution of charged-particle tracking of current detectors. Their properties are calculable in pQCD using nonperturbative track functions [21].

In collisions of heavy nuclei, jets are generated together with the QGP and interact with it. The interaction of a jet and the QGP, known as jet quenching, generates several observable phenomena: jet yield suppression, jet deflection, and modification of jet substructure [22,23]. Jet quenching has been measured extensively at RHIC and the LHC with multiple observables [24–34], providing unique probes of the structure and dynamics of the QGP [35–38].

Jet scattering in the QGP may elucidate the microscopic structure of the medium and the nature of its constituent quasiparticles, in analogy to Rutherford scattering which revealed the atomic nucleus [39]. Rare, single-hard secondary scattering of a jet off of medium constituents would result in a Coulomb-like power-law tail in the emission spectrum (Molière scattering) [40–43].

Two experimental approaches have been proposed to search for direct evidence of jet–QGP scattering: in-medium deflection of the entire jet, which modifies the acoplanarity distribution [28,29,44], and deflection of a

[*]Full author list given at the end of the Letter.

component of the jet shower, which modifies jet internal structure [40,41]. While significant medium-induced modification to acoplanarity distributions has recently been reported, the dependence of the modification on jet resolution parameter R indicates that it is due predominantly to medium response and energy redistribution, which mask the Molière-scattering signal [44–48]. For substructure observables, the in-medium scattering of jet shower components off of QGP quasiparticles corresponds to a relative increase in the rate of high transverse momentum splittings (high k_T) in the jet shower [40,41]; to date, no search for Molière scattering in the QGP based on jet substructure has been reported.

This Letter reports the first measurement of medium-induced modification of jet substructure using high-k_T splittings to search for quasiparticle scattering in the quark-gluon plasma. The data were recorded by the ALICE Collaboration during LHC Run 2 for pp collisions and for central and semicentral Pb-Pb collisions at center-of-mass energy per nucleon pair $\sqrt{s_{\rm NN}} = 5.02$ TeV. Charged-particle jets are reconstructed using the anti-k_T algorithm [49,50] with resolution parameter $R = 0.2$ in the $60 < p_{T,\rm ch\,jet} < 80$ GeV/c jet transverse momentum interval. Background from the underlying event is corrected using constituent subtraction [51]. Jet substructure is measured using the soft drop [52] and dynamical grooming [53] algorithms. Theoretical calculations incorporating jet quenching are used to assess the effects of in-medium Molière scattering, and are compared to the data.

The ALICE detector and its performance are described in Refs. [5,54,55]. Event triggering and event characterization utilize the V0A and V0C scintillator detectors, which cover pseudorapidity intervals $2.8 < \eta < 5.1$ and $-3.7 < \eta < -1.7$, respectively [56], and the Zero Degree Calorimeters located ± 112.5 m along the beam axis from the nominal interaction point of the beams. Charged-particle tracking is carried out using signals from the Inner Tracking System (ITS) [57] and Time Projection Chamber (TPC) [58] [and Transition Radiation Detector (TRD) [59] in pp collisions]. The tracking acceptance covers $|\eta| < 0.9$ over the full azimuth.

The dataset, triggering, and event selection for pp and Pb-Pb collisions at $\sqrt{s_{\rm NN}} = 5.02$ TeV are identical to those of the analysis described in Ref. [31]. Data were recorded with a minimum bias trigger and an event-activity (EA) trigger based on the V0 signal. For the Pb-Pb analysis, events are selected within the 0%–10% ("central") and 30%–50% ("semicentral") decile bins in EA. After event selection the pp collision dataset comprises 870×10^6 events, corresponding to integrated luminosity $\mathcal{L}_{\rm int} = 18.0 \pm 0.4$ nb^{-1} [60], while the Pb-Pb dataset comprises 92×10^6 central and 90×10^6 semicentral events, corresponding to $\mathcal{L}_{\rm int} = 0.12$ and 0.06 nb^{-1}, respectively, with approximately 3% uncertainty [61].

Charged-particle tracks accepted for the analysis have $p_T > 0.15$ GeV/c. Because of the spatially nonuniform ITS response, which also varied in time during the data-taking period, different classes of tracks are combined to create a population of charged-particle tracks with approximately uniform azimuthal acceptance [62]. Accepted tracks have momentum resolution $\sigma(p_T)/p_T \sim 1\%$ for track $p_T = 1$ GeV/c and 4% for $p_T = 50$ GeV/c.

Both the pp and Pb-Pb datasets are corrected using events simulated by the PYTHIA8 generator [63] with the Monash 2013 tune [64], whose output is denoted "particle level." These events are then passed through a detailed model of the ALICE apparatus using GEANT3 [65] to simulate detector effects, and reconstructed with the same algorithms utilized for the event, track, and jet reconstruction of the data; such events are denoted "detector level." For Pb-Pb collisions, detector-level events are additionally embedded into real Pb-Pb data to include the effect of background from the underlying event, and are referred to as "reconstructed level."

Measurements in pp collisions are compared with particle-level calculations using the pp-collision mode of JEWEL [66,67] and the hybrid model [68], which are based on PYTHIA6 [69] and PYTHIA8, respectively, and the JETSCAPE PP19 tune [70] based on the vacuum mode of the MATTER model [71]. For Pb-Pb collisions, the data are compared to calculations incorporating jet quenching. JETSCAPE (v3.5 AA22 tune [72–74]) provides a multistage calculation of medium-modified parton showers with virtuality-dependent interactions, based on MATTER and LBT [75]. The hybrid model [41,76] incorporates AdS-CFT-inspired partonic energy loss and a model of medium response ("wake"). JEWEL is based on the BDMPS energy loss formalism [77] within a medium modeled by Bjorken expansion, with an option to explicitly account for the distribution of partons in the QGP that recoil from the jet-QGP interaction. JETSCAPE and JEWEL include Molière scattering, while the hybrid model can disable elastic $2 \to 2$ Molière scattering to isolate such scattering effects.

The large underlying-event (UE) background in measured data is characterized via the p_T density ρ and mass density $\rho_{\rm m}$ [33,62]. This background is suppressed using event-by-event constituent subtraction [51] with maximum subtraction distance parameter $R_{\rm max} = 0.1$, and p_T weight $\alpha = 0$, which is applied prior to jet finding. No UE subtraction is applied in pp collisions. Jet clustering implemented in FastJet 3.3.3 [78] is carried out twice in each event: first applying the anti-k_T clustering algorithm [49,50] with charged-particle tracks to reconstruct jet candidates, and then using the Cambridge-Aachen (CA) clustering algorithm [79] with jet constituents from selected jet candidates to examine the jet substructure.

The anti-k_T clustering utilizes jet resolution parameter $R = 0.2$ and the E-recombination scheme [49]. The value $R = 0.2$ was chosen as a balance between sensitivity to medium effects and measurement precision in the complex heavy-ion collision environment. The pion mass is assumed for all tracks. Charged-particle jet candidates are required to have $40 \leq p_{T,\text{ch jet}} < 120\ \text{GeV}/c$, jet area $A_{\text{jet}} > 0.6\pi R^2$ [80], and jet centroid $|\eta_{\text{jet}}| < 0.9 - R$, with the minimum $p_{T,\text{ch jet}}$ and area requirements applied to remove jet candidates arising from uncorrelated background. Jet candidates containing a constituent with $p_T > 100\ \text{GeV}/c$ are rejected due to reduced momentum resolution in this region. After background subtraction, the area and constituent p_T requirements remove fewer than 1% of all jets.

Jet grooming algorithms [81,82] are used to remove soft, wide-angle radiation by unwinding the CA recombination tree, allowing the identification of hard splittings. At each recombination step the algorithm evaluates a specified grooming condition based on a "hardness measure," either accepting and recording the splitting properties, or rejecting the splitting and following the harder subjet to the next splitting. We utilize two different grooming algorithms which select splittings in distinct but partially overlapping regions of phase space, which may probe Molière scattering in different ways.

For soft drop grooming (SD) [52], the hardness measure is the fraction of the momentum carried in the softer subjet, z, and the grooming condition is $z > z_{\text{cut}}(\Delta R/R)^{\beta}$, where ΔR is the angle between the subjets, and z_{cut} and β are parameters of the algorithm. Successive splittings are evaluated until one passes the grooming condition, which tags the event, or no splittings remain (untagged event). This analysis utilizes $z_{\text{cut}} = 0.2$ and $\beta = 0$ to preferentially select more symmetric splittings.

For dynamical grooming (DyG) [53], the hardness measure is $\kappa \propto z(1-z)p_{\text{T,split}}(\Delta R/R)^{a}$, where a is a tunable hardness parameter and $p_{T,\text{split}}$ is the transverse momentum of the parent splitting. There is no explicit grooming condition, in contrast to SD; rather, the splitting with the largest value of hardness measure is always selected. This analysis utilizes $a = 1.0$ to preferentially select high-k_T splittings which may not be selected by SD [83].

Single hard scatterings may generate hard parton shower splittings. In this analysis, jet grooming is used to search for such hard splittings using the distribution of the relative transverse momentum of each splitting,

$$k_T = p_{T,\text{subleading}} \sin \Delta R, \tag{1}$$

where $p_{T,\text{subleading}}$ is the transverse momentum of the softer subjet, $\Delta R = \sqrt{\Delta y^2 + \Delta\varphi^2}$, and $\Delta\varphi$ and Δy are the subjet azimuthal angle and rapidity difference. The splitting phase space is characterized by k_T and ΔR, which are used to construct the Lund plane [84], and can be related by the momentum sharing fraction. The value of the splitting selected by the grooming algorithm is denoted $k_{T,g}$.

The complex background in Pb-Pb collisions generates false jet shower branches that may mask physical jet splittings and the physical leading and subleading subjets, with the subleading subjet more susceptible to contamination [31,85]. The probability to falsely tag a background splitting is determined using embedding [85]. Measurements with small R in noncentral Pb-Pb collisions mitigate such effects.

The DyG algorithm is especially susceptible to selecting incorrectly identified subjets since it considers all iterative splittings, without imposing a hard cutoff in the grooming condition. This effect is mitigated in the Pb-Pb analysis by requiring $k_{T,g}^{\text{meas}} > 1\ \text{GeV}/c$ in semicentral and $k_{T,g}^{\text{meas}} > 1.5\ \text{GeV}/c$ in central collisions, where $k_{T,g}^{\text{meas}}$ is the background-subtracted but otherwise uncorrected $k_{T,g}$ distribution. This requirement trades more limited kinematic reach for increased purity; for details see Appendix A.

This minimum $k_{T,g}^{\text{meas}}$ requirement and the SD grooming condition similarly reduce soft contamination and improve tagging purity. For central Pb-Pb collisions, SD ($z_{\text{cut}} = 0.2$) and DyG ($a = 1.0$) with $k_{T,g}^{\text{meas}}$ have a subleading subjet true tagging rate of $\sim 80\% - 90\%$.

The $k_{T,g}$ distributions are corrected for background fluctuations and detector effects, including track p_T resolution and tracking inefficiency. A response matrix is constructed in Pb-Pb (pp) collisions by correlating a probe jet at particle level and reconstructed level (detector level), relating the $p_{T,\text{jet}}$ and $k_{T,g}$ distributions. The response matrix is used to perform 2D iterative Bayesian unfolding [86,87] as implemented in RooUnfold [88]. The optimal iteration for unfolding regularization is chosen such that variation in the unfolded distribution for successive iterations is less than 1%. The iteration number for regularization, which is optimized for each grooming method and collision system, ranges from 6 to 11.

For Pb-Pb collisions, systematic uncertainty in the $k_{T,g}$ distribution arises from the unfolding procedure, tracking efficiency, generator dependence of the response matrix, subtraction of the underlying event, and nonclosure of the unfolding procedure due to mistagged subjets. For pp collisions, systematic uncertainty arises from unfolding, tracking efficiency, and generator dependence.

Systematic uncertainties are quantified as described in Appendix B. The systematic uncertainty due to track selection and ITS-TPC track-matching efficiency uncertainty is determined by randomly rejecting tracks with a given probability, which is p_T dependent in Pb-Pb collisions. Under- and oversubtraction of background is assessed by varying the constituent subtraction distance parameter R_{max}. Systematic uncertainties in the unfolding procedure are evaluated by varying the regularization parameter, the minimum jet $p_{T,\text{ch jet}}$ range, the $k_{T,g}$ binning, and the prior. Generator dependence of the corrections is evaluated by unfolding with an alternative response matrix constructed using HERWIG7 [89,90] in

pp collisions and JEWEL without recoils in Pb-Pb collisions.

A closure test that varies analysis components with respect to their nominal values is utilized to assess the full analysis chain. Closure corresponds to consistency within statistical error of corrected spectra for the variant and nominal components. Component variations are used to assess systematic uncertainties and analysis consistency, such as the sensitivity to the prior spectrum shape, as well as the residual background contribution via embedding and a parametrized thermal model. Point-by-point excursions from the closure tests beyond 1σ statistical error contribute to the systematic uncertainty. Closure tests to access the impact of residual background contamination exhibit nonclosure of up to 12% in a single bin, with largest nonclosure in central Pb-Pb collisions.

The various contributions to the systematic uncertainty are largely uncorrelated among each other and are added in quadrature. The cumulative systematic uncertainty has magnitude 8%–32% for central Pb-Pb and 2%–7% for pp collisions. The dominant uncertainties arise from the generator dependence of the corrections, subtraction, and nonclosure for Pb-Pb collisions, and the generator dependence and tracking for pp collisions.

Figure 1 shows the corrected $k_{T,g}$ yield distributions measured in pp and in central and semicentral Pb-Pb collisions, using DyG ($a = 1.0$) (left) and SD ($z_{\rm cut} = 0.2$) (right). Each distribution is normalized by the number of jets found in the $60 < p_{T,\rm ch\,jet} < 80$ GeV$/c$ interval. This is the first measurement of heavy-ion collision data to employ DyG. All distributions have a similar shape, with a steeply decreasing slope for $k_{T,g} > 1$ GeV$/c$. The results from pp collisions show a maximum at $k_{T,g} \approx 0.5$–1 GeV$/c$. The DyG ($a = 1.0$) spectra in Pb-Pb collisions are restricted to $k_{T,g} > 2$ GeV$/c$ ($k_{T,g} > 3$ GeV$/c$) in semicentral (central) collisions due to the minimum $k_{T,g}$ requirement discussed above. The SD ($z_{\rm cut} = 0.2$) spectra from pp collisions exhibit larger yield at high $k_{T,g}$ than those from Pb-Pb collisions, while for DyG ($a = 1.0$), the pp and Pb-Pb spectra are consistent within uncertainties for $k_{T,g} > 2$ GeV$/c$ where the Pb-Pb results are available. Comparing at fixed centrality and collision system, the DyG ($a = 1.0$) and SD ($z_{\rm cut} = 0.2$) distributions are consistent over the measured $k_{T,g}$ range within the systematic error and statistical uncertainty.

Figure 2 shows the same distributions as Fig. 1, in this case as the ratio with a smooth function that parametrizes the data (details in Appendix C). This representation removes the main functional dependence on $k_{T,g}$ so that detailed variation of the distributions can be seen. The function parameters are different for each collision system, centrality class, and grooming method. Model calculations are also shown, and are divided by the same data parametrization. In the upper panels, the central values of the JETSCAPE and hybrid model calculations tend to underpredict the measured pp distribution at high k_T for both DyG ($a = 1.0$) and SD ($z_{\rm cut} = 0.2$), though are consistent with the data within the uncertainties. At low $k_{T,g}$ (< 1 GeV$/c$), the JETSCAPE and hybrid calculations with

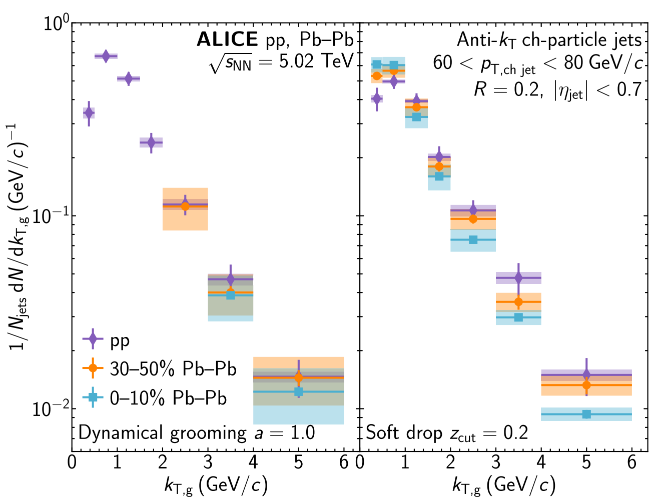

FIG. 1. Unfolded $k_{T,g}$ spectra for splittings selected by dynamical grooming $a = 1.0$ (left) and soft drop $z_{\rm cut} = 0.2$ (right) in pp and semicentral and central Pb-Pb collisions. The jets are measured with $R = 0.2$ in the $60 < p_{T,\rm ch\,jet} < 80$ GeV$/c$ interval. Statistical uncertainties are represented by bars, while systematic uncertainties are shown in shaded boxes.

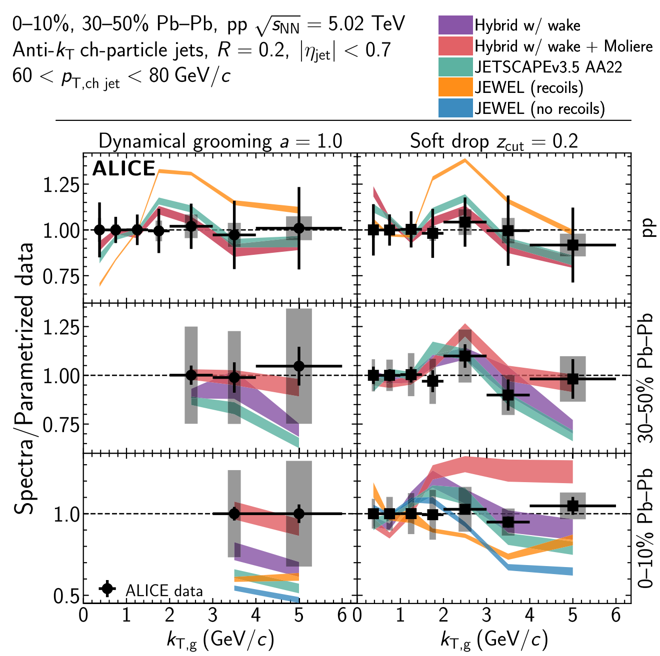

FIG. 2. Ratio of $k_{T,g}$ distributions for data and model calculations to a smooth parametrization of the data, selected by dynamical grooming $a = 1.0$ (left) and soft drop $z_{\rm cut} = 0.2$ (right). Data points are shown in black, with statistical (error bars) and systematic (gray boxes) uncertainties. The bands for the model calculations show statistical uncertainties.

SD ($z_{\mathrm{cut}} = 0.2$) grooming hint towards slightly overpredicting the data, while JEWEL underpredicts the DyG ($a = 1.0$) data. JEWEL overestimates the data at intermediate $k_{T,g}$ for both grooming methods. For semicentral Pb-Pb collisions, displayed in the middle panels, both the DyG ($a = 1.0$) and SD ($z_{\mathrm{cut}} = 0.2$) measurements are described well by all models for $k_{T,g} < 4$ GeV/c. However, at high $k_{T,g}$, the hybrid model with Molière scattering (Hybrid/Molière) agrees better with the SD ($z_{\mathrm{cut}} = 0.2$) data, while there is a hint that the other models underpredict the measured distributions. The bottom panels show tension of the models and data for SD ($z_{\mathrm{cut}} = 0.2$) in central Pb-Pb collisions. At high $k_{T,g} > 3$ GeV/c, the hybrid model without Molière scattering (Hybrid/noMolière) best describes the data, while Hybrid/Molière overpredicts, JETSCAPE slightly underpredicts, and JEWEL with and without recoils underpredict the measured values. For DyG ($a = 1.0$), Hybrid/Molière and Hybrid/noMolière best describe the data, while JETSCAPE and JEWEL underpredict the ratio. The large systematic uncertainties of the DyG ($a = 1.0$) spectra are due to a strong dependence of the grooming algorithm on the generator used to derive corrections of the spectra, limiting the model discrimination power. This indicates that the additional phase space probed by the algorithm does not provide further resolving power.

In-medium Molière scattering is expected to generate yield enhancement at large $k_{T,g}$ [40,41], as seen in the hybrid model variants in Fig. 2. To search for this effect, Fig. 3 shows the ratios of $k_{T,g}$ distributions for semicentral and central Pb-Pb collisions to that for pp collisions. The SD ($z_{\mathrm{cut}} = 0.2$) distributions exhibit medium-induced yield enhancement for $k_{T,g} < 1$ GeV/c and yield suppression at higher $k_{T,g}$, with stronger medium-induced effects in central than in semicentral Pb-Pb collisions. The DyG ($a = 1.0$) distributions hint at yield suppression at large $k_{T,g}$ for central Pb-Pb collisions but not for semicentral Pb-Pb collisions, though the ratios in both cases are consistent with unity within the systematic uncertainties. Since yield suppression is observed in the data in the high-$k_{T,g}$ region, this measurement does not show direct evidence of in-medium Molière scattering. The SD ($z_{\mathrm{cut}} = 0.2$) analysis for central Pb-Pb collisions (Fig. 3, lower right) exhibits the most significant medium-induced modifications in this analysis, with experimental uncertainties which provide the best discrimination of model predictions. We therefore focus primarily on these data for detailed model comparisons and physics conclusions.

For SD ($z_{\mathrm{cut}} = 0.2$) the central Pb-Pb/pp yield ratio is smaller than unity (where unity corresponds to the null hypothesis) by 2.7σ for $3 < k_{T,g} < 4$ GeV/c and by 2.4σ for $4 < k_{T,g} < 6$ GeV/c based on a quadrature sum of the statistical error and systematic uncertainty. This medium-induced narrowing of jet structure is qualitatively consistent

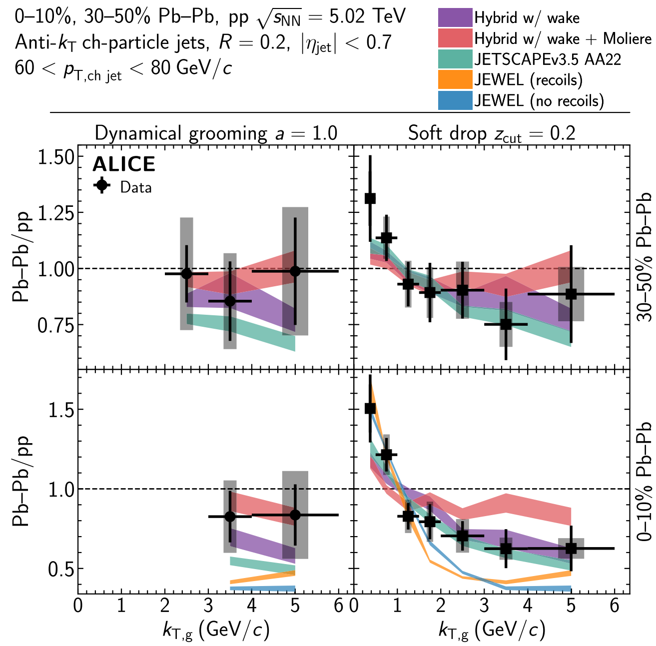

FIG. 3. Ratio of the $k_{T,g}$ distributions measured in Pb-Pb and pp collisions for dynamical grooming $a = 1.0$ (left) and SD ($z_{\mathrm{cut}} = 0.2$) (right), with comparison to model calculations. Statistical uncertainties are shown as error bars and systematic uncertainties are shown as gray shaded boxes for the measured ratios. The width of the colored bands corresponds to the statistical uncertainties in the model calculations.

with effects found in other inclusive jet substructure measurements [30,31,91], including the trend given by the combination of the groomed jet radius and momentum sharing. Such narrowing is commonly interpreted as selection bias which modifies the relative fraction of quark- or gluon-originating jets, due to the combined effects of a falling p_T spectrum and larger energy loss in the medium for wider jets [92–95]. The smaller modification of the $k_{T,g}$ distribution observed in semicentral Pb-Pb collisions is consistent with this picture, due to the correspondingly smaller jet energy loss in that population. The single-hard scattering signature may also be suppressed by subsequent multiple soft interactions with the medium, which smear the angular correlations of jet constituents, such that the Molière scattering is not reconstructed [96]. Medium modification of coherence length [76,97] and of emission formation time [98] may also explain the measured narrowing.

Figure 3 also shows model calculations. None of the models describe all measured distributions in Figs. 2 and 3, with different levels of agreement for the two grooming algorithms. The central Pb-Pb data (lower right) are well-described within uncertainties by JETSCAPE (with Molière scattering) and Hybrid/noMolière, but not by Hybrid/Molière or either variant of JEWEL. From this comparison it is evident that the different theoretical approaches of these models to jet quenching and the bulk dynamics of the

QGP generate markedly different predictions for the relative effect of Molière scattering, which these and other complementary measurements [44] can discriminate. Further exploration of the key model features underlying these differences requires a dedicated global analysis of the world's jet quenching data (e.g., [37]).

This Letter reports the first measurement of the distribution of the hardest relative transverse jet splitting, $k_{T,g}$, in pp and Pb-Pb collisions, to search for evidence of quasiparticle scattering in the quark-gluon plasma. The hardest splitting is identified using the soft drop and dynamical grooming algorithms, the latter for the first time in heavy-ion collisions. The high-$k_{T,g}$ yield in central Pb-Pb collisions is observed to be suppressed relative to that in pp collisions, consistent with in-medium narrowing effects seen in other jet substructure observables. No direct evidence is observed for in-medium quasiparticle scattering within the measured phase space. Model calculations can reproduce the measurements within uncertainties, but differ in the necessity to include quasiparticle scattering effects in order to do so. In these models, the Molière scattering signal may be masked by yield suppression due to jet energy loss, with their relative effects depending upon the theoretical picture underlying the modeling of jet quenching, bulk dynamics, and the vacuum parton shower. These data therefore provide new constraints on theoretical modeling of the microscopic structure and dynamics of the quark-gluon plasma.

Acknowledgments—We gratefully acknowledge Zach Hulcher and Daniel Pablos, and Yasuki Tachibana and the JETSCAPE Collaboration, for providing calculations. The ALICE Collaboration would like to thank all its engineers and technicians for their invaluable contributions to the construction of the experiment and the CERN accelerator teams for the outstanding performance of the LHC complex. The ALICE Collaboration gratefully acknowledges the resources and support provided by all Grid centers and the Worldwide LHC Computing Grid (WLCG) collaboration. The ALICE Collaboration acknowledges the following funding agencies for their support in building and running the ALICE detector: A. I. Alikhanyan National Science Laboratory (Yerevan Physics Institute) Foundation (ANSL), State Committee of Science and World Federation of Scientists (WFS), Armenia; Austrian Academy of Sciences, Austrian Science Fund (FWF): [Grant DOI: 10.55776/M 2467-N36] and Nationalstiftung für Forschung, Technologie und Entwicklung, Austria; Ministry of Communications and High Technologies, National Nuclear Research Center, Azerbaijan; Conselho Nacional de Desenvolvimento Científico e Tecnológico (CNPq), Financiadora de Estudos e Projetos (Finep), Fundação de Amparo à Pesquisa do Estado de São Paulo (FAPESP) and Universidade Federal do Rio Grande do Sul (UFRGS), Brazil; Bulgarian Ministry of Education and Science, within the National Roadmap for Research Infrastructures 2020-2027 (object CERN), Bulgaria; Ministry of Education of China (MOEC), Ministry of Science & Technology of China (MSTC) and National Natural Science Foundation of China (NSFC), China; Ministry of Science and Education and Croatian Science Foundation, Croatia; Centro de Aplicaciones Tecnológicas y Desarrollo Nuclear (CEADEN), Cubaenergía, Cuba; Ministry of Education, Youth and Sports of the Czech Republic, Czech Republic; The Danish Council for Independent Research | Natural Sciences, the VILLUM FONDEN and Danish National Research Foundation (DNRF), Denmark; Helsinki Institute of Physics (HIP), Finland; Commissariat à l'Energie Atomique (CEA) and Institut National de Physique Nucléaire et de Physique des Particules (IN2P3) and Centre National de la Recherche Scientifique (CNRS), France; Bundesministerium für Bildung und Forschung (BMBF) and GSI Helmholtzzentrum für Schwerionenforschung GmbH, Germany; General Secretariat for Research and Technology, Ministry of Education, Research and Religions, Greece; National Research, Development and Innovation Office, Hungary; Department of Atomic Energy Government of India (DAE), Department of Science and Technology, Government of India (DST), University Grants Commission, Government of India (UGC) and Council of Scientific and Industrial Research (CSIR), India; National Research and Innovation Agency—BRIN, Indonesia; Istituto Nazionale di Fisica Nucleare (INFN), Italy; Japanese Ministry of Education, Culture, Sports, Science and Technology (MEXT) and Japan Society for the Promotion of Science (JSPS) KAKENHI, Japan; Consejo Nacional de Ciencia (CONACYT) y Tecnología, through Fondo de Cooperación Internacional en Ciencia y Tecnología (FONCICYT) and Dirección General de Asuntos del Personal Academico (DGAPA), Mexico; Nederlandse Organisatie voor Wetenschappelijk Onderzoek (NWO), Netherlands; The Research Council of Norway, Norway; Pontificia Universidad Católica del Perú, Peru; Ministry of Science and Higher Education, National Science Centre and WUT ID-UB, Poland; Korea Institute of Science and Technology Information and National Research Foundation of Korea (NRF), Republic of Korea; Ministry of Education and Scientific Research, Institute of Atomic Physics, Ministry of Research and Innovation and Institute of Atomic Physics and Universitatea Nationala de Stiinta si Tehnologie Politehnica Bucuresti, Romania; Ministry of Education, Science, Research and Sport of the Slovak Republic, Slovakia; National Research Foundation of South Africa, South Africa; Swedish Research Council (VR) and Knut & Alice Wallenberg Foundation (KAW), Sweden; European Organization for Nuclear Research, Switzerland; Suranaree University of Technology (SUT), National Science and

Technology Development Agency (NSTDA) and National Science, Research and Innovation Fund (NSRF via PMU-B B05F650021), Thailand; Turkish Energy, Nuclear and Mineral Research Agency (TENMAK), Turkey; National Academy of Sciences of Ukraine, Ukraine; Science and Technology Facilities Council (STFC), United Kingdom; National Science Foundation of the USA (NSF) and U.S. Department of Energy, Office of Nuclear Physics (DOE NP), USA. In addition, individual groups or members have received support from: Czech Science Foundation (Grant No. 23-07499S), Czech Republic; FORTE project, Reg. No. CZ.02.01.01/00/22_008/0004632, Czech Republic, co-funded by the European Union, Czech Republic; European Research Council (Grant No. 950692), European Union; ICSC—Centro Nazionale di Ricerca in High Performance Computing, Big Data and Quantum Computing, European Union—NextGenerationEU; Academy of Finland (Center of Excellence in Quark Matter) (Grants No. 346327, No. 346328), Finland.

[1] J. C. Collins and M. J. Perry, Superdense matter: Neutrons or asymptotically free quarks?, Phys. Rev. Lett. **34**, 1353 (1975).

[2] E. V. Shuryak, Theory of hadronic plasma, Sov. Phys. JETP **47**, 212 (1978).

[3] J. Adams *et al.* (STAR Collaboration), Experimental and theoretical challenges in the search for the quark gluon plasma: The STAR Collaboration's critical assessment of the evidence from RHIC collisions, Nucl. Phys. **A757**, 102 (2005).

[4] K. Adcox *et al.* (PHENIX Collaboration), Formation of dense partonic matter in relativistic nucleus-nucleus collisions at RHIC: Experimental evaluation by the PHENIX Collaboration, Nucl. Phys. **A757**, 184 (2005).

[5] S. Acharya *et al.* (ALICE Collaboration), The ALICE experiment—A journey through QCD, Eur. Phys. J. C **84**, 813 (2024).

[6] A. Hayrapetyan *et al.* (CMS Collaboration), Overview of high-density QCD studies with the CMS experiment at the LHC, Phys. Rep. **1115**, 219 (2025).

[7] B. V. Jacak and B. Müller, The exploration of hot nuclear matter, Science **337**, 310 (2012).

[8] W. Busza, K. Rajagopal, and W. van der Schee, Heavy ion collisions: The big picture, and the big questions, Annu. Rev. Nucl. Part. Sci. **68**, 339 (2018).

[9] J. W. Harris and B. Müller, 'QGP signatures' revisited, Eur. Phys. J. C **84**, 247 (2023).

[10] C. Ratti, Lattice QCD and heavy ion collisions: A review of recent progress, Rep. Prog. Phys. **81**, 084301 (2018).

[11] J. N. Guenther, Overview of the QCD phase diagram—recent progress from the lattice, Eur. Phys. J. A **57**, 136 (2021).

[12] B. Abelev *et al.* (ALICE Collaboration), Measurement of the inclusive differential jet cross section in pp collisions at $\sqrt{s} = 2.76$ TeV, Phys. Lett. B **722**, 262 (2013).

[13] G. Aad *et al.* (ATLAS Collaboration), Jet mass and substructure of inclusive jets in $\sqrt{s} = 7$ TeV pp collisions with the ATLAS experiment, J. High Energy Phys. 05 (2012) 128.

[14] A. Tumasyan *et al.* (CMS Collaboration), Measurement and QCD analysis of double-differential inclusive jet cross sections in proton-proton collisions at $\sqrt{s} = 13$ TeV, J. High Energy Phys. 02 (2022) 142.

[15] G. Aad *et al.* (ATLAS Collaboration), Measurement of the Lund jet plane using charged particles in 13 TeV proton-proton collisions with the ATLAS detector, Phys. Rev. Lett. **124**, 222002 (2020).

[16] S. Acharya *et al.* (ALICE Collaboration), Measurements of the groomed jet radius and momentum splitting fraction with the soft drop and dynamical grooming algorithms in pp collisions at $\sqrt{s} = 5.02$ TeV, J. High Energy Phys. 05 (2023) 244.

[17] B. Abelev *et al.* (STAR Collaboration), Longitudinal double-spin asymmetry and cross section for inclusive jet production in polarized proton collisions at $\sqrt{s} = 200$ GeV, Phys. Rev. Lett. **97**, 252001 (2006).

[18] L. Adamczyk *et al.* (STAR Collaboration), Measurement of the cross section and longitudinal double-spin asymmetry for di-jet production in polarized pp collisions at $\sqrt{s} = 200$ GeV, Phys. Rev. D **95**, 071103 (2017).

[19] G. Aad *et al.* (ATLAS Collaboration), Measurement of the inclusive jet cross-section in proton-proton collisions at $\sqrt{s} = 7$ TeV using 4.5 fb^{-1} of data with the ATLAS detector, J. High Energy Phys. 02 (2015) 153.

[20] V. Khachatryan *et al.* (CMS Collaboration), Measurement and QCD analysis of double-differential inclusive jet cross-sections in pp collisions at $\sqrt{s} = 8$ TeV and ratios to 2.76 and 7 TeV, J. High Energy Phys. 03 (2017) 156.

[21] K. Lee, I. Moult, F. Ringer, and W. J. Waalewijn, A formalism for extracting track functions from jet measurements, J. High Energy Phys. 01 (2024) 194.

[22] L. Cunqueiro and A. M. Sickles, Studying the QGP with jets at the LHC and RHIC, Prog. Part. Nucl. Phys. **124**, 103940 (2022).

[23] L. Apolinário, Y.-J. Lee, and M. Winn, Heavy quarks and jets as probes of the QGP, Prog. Part. Nucl. Phys. **127**, 103990 (2022).

[24] J. Adam *et al.* (STAR Collaboration), Measurement of inclusive charged-particle jet production in Au + Au collisions at $\sqrt{s_{NN}} = 200$ GeV, Phys. Rev. C **102**, 054913 (2020).

[25] S. Acharya *et al.* (ALICE Collaboration), Measurement of the radius dependence of charged-particle jet suppression in Pb–Pb collisions at $\sqrt{s_{\mathrm{NN}}} = 5.02$ TeV, Phys. Lett. B **849**, 138412 (2024).

[26] M. Aaboud *et al.* (ATLAS Collaboration), Measurement of the nuclear modification factor for inclusive jets in Pb + Pb collisions at $\sqrt{s_{\mathrm{NN}}} = 5.02$ TeV with the ATLAS detector, Phys. Lett. B **790**, 108 (2019).

[27] A. M. Sirunyan *et al.* (CMS Collaboration), First measurement of large area jet transverse momentum spectra in heavy-ion collisions, J. High Energy Phys. 05 (2021) 284.

[28] J. Adam *et al.* (ALICE Collaboration), Measurement of jet quenching with semi-inclusive hadron-jet distributions in central Pb–Pb collisions at $\sqrt{s_{\mathrm{NN}}} = 2.76$ TeV, J. High Energy Phys. 09 (2015) 170.

[29] L. Adamczyk *et al.* (STAR Collaboration), Measurements of jet quenching with semi-inclusive hadron + jet distributions in Au + Au collisions at $\sqrt{s_{NN}} = 200$ GeV, Phys. Rev. C **96**, 024905 (2017).

[30] G. Aad *et al.* (ATLAS Collaboration), Measurement of substructure-dependent jet suppression in Pb + Pb collisions at 5.02 TeV with the ATLAS detector, Phys. Rev. C **107**, 054909 (2023).

[31] S. Acharya *et al.* (ALICE Collaboration), Measurement of the groomed jet radius and momentum splitting fraction in pp and Pb–Pb collisions at $\sqrt{s_{\rm NN}} = 5.02$ TeV, Phys. Rev. Lett. **128**, 102001 (2022).

[32] A. M. Sirunyan *et al.* (CMS Collaboration), Measurement of the groomed jet mass in PbPb and pp collisions at $\sqrt{s_{\rm NN}} = 5.02$ TeV, J. High Energy Phys. 10 (2018) 161.

[33] S. Acharya *et al.* (ALICE Collaboration), First measurement of jet mass in Pb–Pb and p–Pb collisions at the LHC, Phys. Lett. B **776**, 249 (2018).

[34] G. Aad *et al.* (ATLAS Collaboration), Measurement of suppression of large-radius jets and its dependence on substructure in Pb + Pb collisions at $\sqrt{s_{\rm NN}} = 5.02$ TeV with the ATLAS detector, Phys. Rev. Lett. **131**, 172301 (2023).

[35] K. M. Burke *et al.* (JET Collaboration), Extracting the jet transport coefficient from jet quenching in high-energy heavy-ion collisions, Phys. Rev. C **90**, 014909 (2014).

[36] S. Cao *et al.* (JETSCAPE Collaboration), Determining the jet transport coefficient $\hat{q}$ from inclusive hadron suppression measurements using Bayesian parameter estimation, Phys. Rev. C **104**, 024905 (2021).

[37] R. Ehlers *et al.* (JETSCAPE Collaboration), Bayesian Inference analysis of jet quenching using inclusive jet and hadron suppression measurements, arXiv:2408.08247 [Phys. Rev. C (to be published)].

[38] W. Ke and X.-N. Wang, QGP modification to single inclusive jets in a calibrated transport model, J. High Energy Phys. 05 (2021) 041.

[39] E. Rutherford, The scattering of α and β particles by matter and the structure of the atom, Phil. Mag. Ser. 6 **21**, 669 (1911).

[40] F. D'Eramo, M. Lekaveckas, H. Liu, and K. Rajagopal, Momentum broadening in weakly coupled quark-gluon plasma (with a view to finding the quasiparticles within liquid quark-gluon plasma), J. High Energy Phys. 05 (2013) 031.

[41] F. D'Eramo, K. Rajagopal, and Y. Yin, Molière scattering in quark-gluon plasma: Finding point-like scatterers in a liquid, J. High Energy Phys. 01 (2019) 172.

[42] J. Barata, Y. Mehtar-Tani, A. Soto-Ontoso, and K. Tywoniuk, Revisiting transverse momentum broadening in dense QCD media, Phys. Rev. D **104**, 054047 (2021).

[43] L. Cunqueiro, D. Pablos, A. Soto-Ontoso, M. Spousta, A. Takacs, and M. Verweij, Isolating perturbative QCD splittings in heavy-ion collisions, Phys. Rev. D **110**, 014015 (2024).

[44] S. Acharya *et al.* (ALICE Collaboration), Observation of medium-induced yield enhancement and acoplanarity broadening of low-$p_{\rm T}$ jets from measurements in pp and central Pb–Pb collisions at $\sqrt{s_{\rm NN}} = 5.02$ TeV, Phys. Rev. Lett. **133**, 022301 (2024).

[45] S. Acharya *et al.* (ALICE Collaboration), Measurements of jet quenching using semi-inclusive hadron + jet distributions in pp and central Pb–Pb collisions at $\sqrt{s_{\rm NN}} = 5.02$ TeV, Phys. Rev. C **110**, 014906 (2024).

[46] M. Abdulhamid *et al.* (STAR Collaboration), Semi-inclusive direct photon + jet and π^0 + jet correlations measured in $p+p$ and central Au + Au collisions at $\sqrt{s_{\rm NN}} = 200$ GeV, arXiv:2309.00145 [Phys. Rev. C (to be published).]

[47] M. Abdulhamid *et al.* (STAR Collaboration), Measurement of in-medium jet modification using direct photon + jet and π^0 + jet correlations in $p+p$ and central Au + Au collisions at $\sqrt{s_{\rm NN}} = 200$ GeV, arXiv:2309.00156 [Phys. Rev. Lett. (to be published)].

[48] A. M. Sirunyan *et al.* (CMS Collaboration), Study of jet quenching with isolated-photon+jet correlations in PbPb and pp collisions at $\sqrt{s_{\rm NN}} = 5.02$ TeV, Phys. Lett. B **785**, 14 (2018).

[49] M. Cacciari, G. P. Salam, and G. Soyez, The catchment area of jets, J. High Energy Phys. 04 (2008) 005.

[50] M. Cacciari, G. P. Salam, and G. Soyez, The anti-k_t jet clustering algorithm, J. High Energy Phys. 04 (2008) 063.

[51] P. Berta, M. Spousta, D. W. Miller, and R. Leitner, Particle-level pileup subtraction for jets and jet shapes, J. High Energy Phys. 06 (2014) 092.

[52] A. J. Larkoski, S. Marzani, G. Soyez, and J. Thaler, Soft Drop, J. High Energy Phys. 05 (2014) 146.

[53] Y. Mehtar-Tani, A. Soto-Ontoso, and K. Tywoniuk, Dynamical grooming of QCD jets, Phys. Rev. D **101**, 034004 (2020).

[54] K. Aamodt *et al.* (ALICE Collaboration), The ALICE experiment at the CERN LHC, J. Instrum. **3**, S08002 (2008).

[55] B. B. Abelev *et al.* (ALICE Collaboration), Performance of the ALICE Experiment at the CERN LHC, Int. J. Mod. Phys. A **29**, 1430044 (2014).

[56] E. Abbas *et al.* (ALICE Collaboration), Performance of the ALICE VZERO system, J. Instrum. **8**, P10016 (2013),

[57] K. Aamodt *et al.* (ALICE Collaboration), Alignment of the ALICE inner tracking system with cosmic-ray tracks, J. Instrum. **5**, P03003 (2010),

[58] J. Alme *et al.*, The ALICE TPC, a large 3-dimensional tracking device with fast readout for ultra-high multiplicity events, Nucl. Instrum. Methods Phys. Res., Sect. A **622**, 316 (2010).

[59] S. Acharya *et al.* (ALICE Collaboration), The ALICE Transition Radiation Detector: Construction, operation, and performance, Nucl. Instrum. Methods Phys. Res., Sect. A **881**, 88 (2018).

[60] S. Acharya *et al.* (ALICE Collaboration), ALICE 2017 luminosity determination for pp collisions at $\sqrt{s} = 5$ TeV, http://cds.cern.ch/record/2648933.

[61] S. Acharya *et al.* (ALICE Collaboration), ALICE luminosity determination for Pb–Pb collisions at $\sqrt{s_{\rm NN}} = 5.02$ TeV, J. Instrum. **19**, P02039 (2024).

[62] B. Abelev *et al.* (ALICE Collaboration), Measurement of event background fluctuations for charged particle jet

reconstruction in Pb–Pb collisions at $\sqrt{s_{NN}} = 2.76$ TeV, J. High Energy Phys. 03 (2012) 053.
[63] T. Sjostrand *et al.*, An introduction to PYTHIA 8.2, Comput. Phys. Commun. **191**, 159 (2015).
[64] P. Skands, S. Carrazza, and J. Rojo, Tuning PYTHIA 8.1: The Monash 2013 tune, Eur. Phys. J. C **74**, 3024 (2014).
[65] R. Brun *et al.*, *GEANT: Detector Description and Simulation Tool; Oct 1994*, CERN Program Library (CERN, Geneva, 1993), Long Writeup W5013, https://cds.cern.ch/record/1082634.
[66] K. C. Zapp, F. Krauss, and U. A. Wiedemann, A perturbative framework for jet quenching, J. High Energy Phys. 03 (2013) 080.
[67] K. C. Zapp, JEWEL 2.0.0—directions for use, Eur. Phys. J. C **74**, 2762 (2014).
[68] J. Casalderrey-Solana, D. C. Gulhan, J. G. Milhano, D. Pablos, and K. Rajagopal, A hybrid strong/weak coupling approach to jet quenching, J. High Energy Phys. 10 (2014) 019.
[69] T. Sjostrand, S. Mrenna, and P. Skands, PYTHIA 6.4 physics and manual, J. High Energy Phys. 05 (2006) 026.
[70] A. Kumar *et al.* (JETSCAPE Collaboration), The JETSCAPE framework: $p+p$ results, Phys. Rev. C **102**, 054906 (2020).
[71] S. Cao and A. Majumder, Nuclear modification of leading hadrons and jets within a virtuality ordered parton shower, Phys. Rev. C **101**, 024903 (2020).
[72] J. Putschke *et al.* (JETSCAPE Collaboration), The JETSCAPE framework, arXiv:1903.07706.
[73] A. Kumar *et al.* (JETSCAPE Collaboration), Inclusive jet and hadron suppression in a multistage approach, Phys. Rev. C **107**, 034911 (2023).
[74] Y. Tachibana *et al.* (JETSCAPE Collaboration), Hard jet substructure in a multi-stage approach, Phys. Rev. C **110**, 044907 (2024).
[75] Y. He, T. Luo, X.-N. Wang, and Y. Zhu, Linear Boltzmann transport for jet propagation in the quark-gluon plasma: Elastic processes and medium recoil, Phys. Rev. C **91**, 054908 (2015).
[76] Z. Hulcher, D. Pablos, and K. Rajagopal, Resolution effects in the hybrid strong/weak coupling model, J. High Energy Phys. 03 (2018) 010.
[77] R. Baier, Y. L. Dokshitzer, A. H. Mueller, S. Peigne, and D. Schiff, Radiative energy loss of high energy quarks and gluons in a finite-volume quark-gluon plasma, Nucl. Phys. **B483**, 291 (1997).
[78] M. Cacciari, G. P. Salam, and G. Soyez, FastJet user manual, Eur. Phys. J. C **72**, 1896 (2012).
[79] Y. L. Dokshitzer, G. D. Leder, S. Moretti, and B. R. Webber, Better jet clustering algorithms, J. High Energy Phys. 08 (1997) 001.
[80] B. Abelev *et al.* (ALICE Collaboration), Measurement of charged jet suppression in Pb–Pb collisions at $\sqrt{s_{NN}} = 2.76$ TeV, J. High Energy Phys. 03 (2014) 013.
[81] Y.-T. Chien and I. Vitev, Probing the hardest branching of jets in heavy ion collisions, Phys. Rev. Lett. **119**, 112301 (2017).
[82] Y. Mehtar-Tani and K. Tywoniuk, Groomed jets in heavy-ion collisions: Sensitivity to medium-induced bremsstrahlung, J. High Energy Phys. 04 (2017) 125.
[83] P. Caucal, A. Soto-Ontoso, and A. Takacs, Dynamically groomed jet radius in heavy-ion collisions, Phys. Rev. D **105**, 114046 (2022).
[84] H. A. Andrews *et al.*, Novel tools and observables for jet physics in heavy-ion collisions, J. Phys. G **47**, 065102 (2020).
[85] J. Mulligan and M. Ploskon, Identifying groomed jet splittings in heavy-ion collisions, Phys. Rev. C **102**, 044913 (2020).
[86] G. D'Agostini, A multidimensional unfolding method based on Bayes' theorem, Nucl. Instrum. Methods Phys. Res., Sect. A **362**, 487 (1995).
[87] G. D'Agostini, Improved iterative Bayesian unfolding, in *Alliance Workshop on Unfolding and Data Correction* (2010), arXiv:1010.0632.
[88] T. Adye, Unfolding algorithms and tests using RooUnfold, in *PHYSTAT 2011* (CERN, Geneva, 2011), pp. 313–318, arXiv:1105.1160.
[89] M. Bahr *et al.*, HERWIG++ physics and manual, Eur. Phys. J. C **58**, 639 (2008).
[90] J. Bellm *et al.*, HERWIG7.0/HERWIG++ 3.0 release note, Eur. Phys. J. C **76**, 196 (2016).
[91] S. Acharya *et al.* (ALICE Collaboration), Measurement of the angle between jet axes in Pb–Pb collisions at $\sqrt{s_{NN}} = 5.02$ TeV, arXiv:2303.13347.
[92] J. Casalderrey-Solana, D. Gulhan, G. Milhano, D. Pablos, and K. Rajagopal, Angular structure of jet quenching within a hybrid strong/weak coupling model, J. High Energy Phys. 03 (2017) 135.
[93] F. Ringer, B.-W. Xiao, and F. Yuan, Can we observe jet p_T-broadening in heavy-ion collisions at the LHC?, Phys. Lett. B **808**, 135634 (2020).
[94] Y.-L. Du, D. Pablos, and K. Tywoniuk, Deep learning jet modifications in heavy-ion collisions, J. High Energy Phys. 21 (2020) 206.
[95] J.-W. Kang, S. Wang, L. Wang, and B.-W. Zhang, Phenomenological study of the angle between jet axes in heavy-ion collisions, Phys. Rev. C **111**, 054905 (2025).
[96] Y. Mehtar-Tani, S. Schlichting, and I. Soudi, Jet thermalization in QCD kinetic theory, J. High Energy Phys. 05 (2023) 091.
[97] J. Casalderrey-Solana, G. Milhano, D. Pablos, and K. Rajagopal, Modification of jet substructure in heavy ion collisions as a probe of the resolution length of quark-gluon plasma, J. High Energy Phys. 01 (2020) 044.
[98] L. Apolinário, P. Guerrero-Rodríguez, and K. Zapp, Exploring the time axis within medium-modified jets, Eur. Phys. J. C **84**, 672 (2024).

End Matter

Appendix A: Subjet purity—The large underlying event present in heavy-ion collisions contaminates the jet shower, leading to potential misidentification of physical jet splittings and the contributing subjets [31,85]. For example, a true leading subjet may be paired with an uncorrelated jet constituent which is coincidentally close in angular phase space, leading to no hard splittings being identified in the declustering tree. Unlike algorithms with a hard cutoff in the grooming condition, DyG requires that a splitting be identified for each measured jet, even in the case that a jet is solely composed of soft splittings. The heavy background contamination of such soft splittings causes unfolding instabilities. These instabilities may be addressed via modifications to existing analysis procedures, which are explored below.

To characterize the impact of background contamination and study mitigation techniques, PYTHIA8 probe jets generated with the Monash 2013 tune are embedded into Pb-Pb data, following a similar evaluation procedure as described in Ref. [85]. The grooming algorithms are applied to the probe jets at both the detector and reconstructed (i.e., embedded) levels. Performance is characterized by the purity, which is the fraction of subjets which are correctly identified in reconstructed-level jets, normalized by the number of groomed subjets found in detector-level jets. Identified splittings and subjets are matched based on subjet constituents, with the reconstructed-level subjet required to carry at least 50% of the detector-level subjet p_T. The leading subjet prong is correctly identified in more than 95% of all splittings, and is not shown here. The subleading subjet prong purity as a function of the detector-level probe $p_{T,\mathrm{ch\,jet}}$ is shown in Fig. 4 for semicentral (left) and central (right) Pb-Pb collisions.

Detector-level $p_{T,\mathrm{ch\,jet}}$ is utilized to assess the impact of background on the purity (as compared to detector effects). The $40 < p_{T,\mathrm{ch\,jet}}^{\mathrm{det}} < 120\ \mathrm{GeV}/c$ interval contains nearly all of the particle-level jets which contribute to the unfolded measurement. Soft drop $z_{\mathrm{cut}} = 0.2$ correctly identifies more than 80% (90%) of subleading prongs in central (semicentral) Pb-Pb collisions. However, the purity drops to 65% (85%) for dynamical grooming $a = 1.0$, which leads to unfolding instabilities.

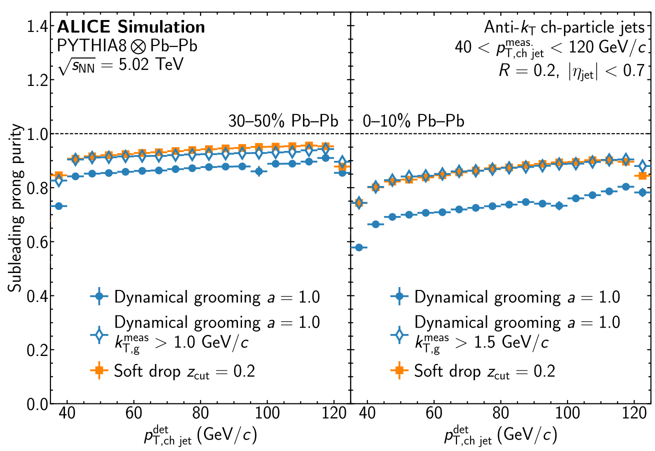

FIG. 4. Subleading subjet purity for soft drop $z_{\mathrm{cut}} = 0.2$ and dynamical grooming $a = 1.0$ applied to jets found in semicentral (left) and central (right) Pb-Pb collisions. Closed markers correspond to the standard grooming algorithms, while open markers represent dynamical grooming $a = 1.0$ with a minimum $k_{T,g}^{\mathrm{meas}}$ requirement. Statistical uncertainties are represented by bars.

The subleading subjet purity can be improved by excluding the most background contaminated region of the $k_{T,g}$ spectra by requiring that the background-subtracted but otherwise uncorrected value, $k_{T,g}^{\mathrm{meas}}$, is larger than a minimum value. Figure 4, open markers, demonstrates this effect, with the subleading subjet purity of dynamical grooming $a = 1.0$ with a minimum $k_{T,g}^{\mathrm{meas}}$ requirement increasing to near agreement with soft drop $z_{\mathrm{cut}} = 0.2$. This requirement causes a corresponding reduction in the kinematic efficiency, which describes the efficiency of finding particle-level jets given a fixed detector-level kinematic interval [80], at low $k_{T,g} \sim 1$–$2\ \mathrm{GeV}/c$. Reduced kinematic efficiency restricts the reported kinematic range to larger $k_{T,g}$ values where the kinematic efficiency is relatively higher, and increases sensitivity to the generator used to correct for this reduction. This analysis requires a kinematic efficiency greater than ∼70%. Optimizing the increase in purity against the reduction in kinematic efficiency (and therefore the reported kinematic range), $k_{T,g}^{\mathrm{meas}} > 1.5(1.0)\ \mathrm{GeV}/c$ in central (semicentral) Pb-Pb collisions was selected for this measurement. The performance of JEWEL without recoils is consistent with the values shown in Fig. 4, indicating limited model sensitivity. Imposing this $k_{T,g}^{\mathrm{meas}}$ condition for soft drop $z_{\mathrm{cut}} = 0.2$ does not improve the subleading subjet purity because the grooming condition already removes the background contamination.

Appendix B: Systematic uncertainties—The systematic uncertainties in this measurement are due to the tracking efficiency ("trk. eff."), the subtraction of the underlying background ("bkgd. sub"), the unfolding procedure, the generator dependence of the unfolding procedure, and the residual nonclosure of the unfolding procedure. Only the tracking, generator dependence, and unfolding apply to the measurement in pp collisions. Sources of uncertainty are evaluated following similar procedures and for similar physical considerations as described in Ref. [31]. Signed uncertainties are symmetrized. The total uncertainty is summed in quadrature over the sources mentioned above, assuming no correlation between the individual uncertainties.

Track selections are considered along with the uncertainty on the ITS–TPC track-matching efficiency to estimate the systematic uncertainty on the observable due to the tracking performance. In pp collisions, this amounts to a p_T-independent uncertainty of ∼3%, while in Pb-Pb collisions, a p_T-dependent parametrization peaks at ∼6% for $p_T = 1\ \mathrm{GeV}/c$ and decreases to ∼3% for $p_T \geq 15\ \mathrm{GeV}/c$. This performance dependence is assessed

TABLE I. Relative systematic uncertainties (%) for $k_{T,g}$ distributions measured using soft drop $z_{\text{cut}} = 0.2$ and dynamical grooming $a = 1.0$ in pp collisions. The minimum and maximum values over the measured $k_{T,g}$ range are reported. The combined uncertainty is the sum in quadrature of the individual uncertainties.

	Relative uncertainty (%)			
pp	Trk. Eff.	Generator	Unfolding	Total
DyG. $a = 1.0$	1%–6%	2%–6%	1%–4%	3%–7%
SD $z_{\text{cut}} = 0.2$	0%–4%	1%–6%	1%–2%	2%–7%

by randomly rejecting tracks according to the magnitude of the uncertainties.

Imperfect background subtraction may bias the $p_{T,\text{ch jet}}$ and k_T dependence of the measured $k_{T,g}$ distributions. The analysis was carried out with two values of the constituent subtraction distance parameter R_{max}, 0.05 and 0.5, to characterize under- and oversubtraction of background contributions. The maximum bin-by-bin variation is assigned as a systematic uncertainty.

Sensitivity to the unfolding procedure is evaluated via variations of the unfolding parameters, including varying the regularization parameter of the Bayesian unfolding by ± 1 unit; increasing and decreasing the minimum smeared jet $p_{T,\text{ch jet}}$ range by ± 5 GeV/c in Pb-Pb collisions (± 3 GeV/c in pp collisions); modifying the $k_{T,g}$ bin edges by up to $\pm 5\%$; and weighing the prior distribution to resemble the uncorrected raw distributions. These variations are correlated in their characterization of the unfolding performance and sensitivity. Consequently, the variations are combined into a single unfolding uncertainty, calculated as the standard deviation of the individual values.

The generator utilized to construct the response matrix used for the unfolding can impact the measured distributions. This is evaluated by constructing alternative response matrices using HERWIG7 [89,90] in pp collisions, and JEWEL 2.2.0 [66,67] without recoils in Pb-Pb collisions. A fast simulation is employed as described in Ref. [31], and the uncertainty is determined as the maximum bin-by-bin variation. The systematic uncertainty derived in central collisions is also applied in semicentral collisions.

To account for the effects of residual subjet misidentifications, two methods are considered. Closure tests are performed using two approaches: (1) unfolding a known input distribution which is weighed to resemble the measured data; and (2) unfolding a known probe distribution which is embedded into a thermal background, as described in Ref. [31]. Any remaining nonclosure in these correction procedures is taken as a systematic uncertainty, with the value assigned as the maximum bin-by-bin difference of the two methods from the nominal value.

Relative systematic uncertainties of $k_{T,g}$ distributions measured using soft drop $z_{\text{cut}} = 0.2$ and dynamical grooming $a = 1.0$ are shown in Table I for pp collisions and Table II for 0%–10% and 30%–50% Pb-Pb collisions.

Appendix C: Parametrization of spectra—A smoothed parametrization was employed in order to factorize the overall features of the spectra while separating out the fluctuations of the data and model calculations. The smoothed functions were separately fit to the data for each grooming method in pp, semicentral, and central Pb-Pb collisions. The same extracted parameters are used in the parametrized function to calculate the ratios with the data and the model calculations. The spectra are parametrized by

$$\begin{aligned} f(k_T, k_T^0, s) = &\{q(k_T, A, B) + [E - q(k_T^0, A, B)]\} \\ &\times t(k_T, k_T^0, -s) \\ &+ \{p(k_T, C, D) + [E - p(k_T^0, C, D)]\} \\ &\times t(k_T, k_T^0, s), \end{aligned} \tag{C1}$$

with each term defined as,

$$\begin{aligned} q(k_T; A, B) &= A(k_T - B)^2, \\ p(k_T; C, D) &= (C k_T)^{-D}, \\ t(k_T; k_T^0, s) &= \{1 + \tanh[(k_T - k_T^0)/s]\}/2, \end{aligned} \tag{C2}$$

where A, B, C, D, and E are fit parameters, $s = 0.25$ GeV/c in pp collisions and $s = 0.1$ GeV/c in Pb-Pb collisions for both grooming methods, and $k_{\text{T}}^0 = 1.25$ GeV/c. For DyG ($a = 1.0$) in semicentral

TABLE II. Relative systematic uncertainties (%) for $k_{T,g}$ distributions measured using soft drop $z_{\text{cut}} = 0.2$ and dynamical grooming $a = 1.0$ in central and semicentral Pb-Pb collisions. The minimum and maximum values over the measured $k_{T,g}$ range are reported. The combined uncertainty is the sum in quadrature of the individual uncertainties.

	Relative uncertainty (%)						
Pb-Pb		Trk. Eff.	Bkgd. Sub.	Unfolding	Generator	Nonclosure	Total
DyG. $a = 1.0$	0%–10%	4%–7%	8%–14%	1%–2%	22%–26%	12%–12%	27%–32%
SD $z_{\text{cut}} = 0.2$	0%–10%	0%–7%	1%–7%	0%–2%	2%–11%	2%–6%	8%–15%
DyG. $a = 1.0$	30%–50%	1%–6%	4%–9%	1%–2%	22%–26%	2%–5%	24%–28%
SD $z_{\text{cut}} = 0.2$	30%–50%	0%–5%	1%–9%	0%–2%	2%–11%	1%–5%	8%–12%

and central Pb-Pb collisions where there are insufficient points to constrain $f(k_T, k_T^0, s)$, the data are fit to $p(k_T; C, D)$ alone. The particular functional forms are arbitrary; they were selected to provide a smooth approximate description of the bulk features of the spectra, with a peak at low $k_{T,g}$ via a quadratic term, transitioning to a power law at high $k_{T,g}$. The $1 + \tanh(\ldots)$ element smoothly transitions between the two terms, while the normalization ensures that each term only contributes in its region of applicability.

S. Acharya,[127] A. Agarwal,[135] G. Aglieri Rinella,[32] L. Aglietta,[24] M. Agnello,[29] N. Agrawal,[25] Z. Ahammed,[135] S. Ahmad,[15] S. U. Ahn,[71] I. Ahuja,[36] A. Akindinov,[140] V. Akishina,[38] M. Al-Turany,[97] D. Aleksandrov,[140] B. Alessandro,[56] H. M. Alfanda,[6] R. Alfaro Molina,[67] B. Ali,[15] A. Alici,[25] N. Alizadehvandchali,[116] A. Alkin,[104] J. Alme,[20] G. Alocco,[24,52] T. Alt,[64] A. R. Altamura,[50] I. Altsybeev,[95] J. R. Alvarado,[44] C. O. R. Alvarez,[44] M. N. Anaam,[6] C. Andrei,[45] N. Andreou,[115] A. Andronic,[126] E. Andronov,[140] V. Anguelov,[94] F. Antinori,[54] P. Antonioli,[51] N. Apadula,[74] L. Aphecetche,[103] H. Appelshäuser,[64] C. Arata,[73] S. Arcelli,[25] R. Arnaldi,[56] J. G. M. C. A. Arneiro,[110] I. C. Arsene,[19] M. Arslandok,[138] A. Augustinus,[32] R. Averbeck,[97] D. Averyanov,[140] M. D. Azmi,[15] H. Baba,[124] A. Badalà,[53] J. Bae,[104] Y. W. Baek,[40] X. Bai,[120] R. Bailhache,[64] Y. Bailung,[48] R. Bala,[91] A. Balbino,[29] A. Baldisseri,[130] B. Balis,[2] Z. Banoo,[91] V. Barbasova,[36] F. Barile,[31] L. Barioglio,[56] M. Barlou,[78] B. Barman,[41] G. G. Barnaföldi,[46] L. S. Barnby,[115] E. Barreau,[103] V. Barret,[127] L. Barreto,[110] C. Bartels,[119] K. Barth,[32] E. Bartsch,[64] N. Bastid,[127] S. Basu,[75] G. Batigne,[103] D. Battistini,[95] B. Batyunya,[141] D. Bauri,[47] J. L. Bazo Alba,[101] I. G. Bearden,[83] C. Beattie,[138] P. Becht,[97] D. Behera,[48] I. Belikov,[129] A. D. C. Bell Hechavarria,[126] F. Bellini,[25] R. Bellwied,[116] S. Belokurova,[140] L. G. E. Beltran,[109] Y. A. V. Beltran,[44] G. Bencedi,[46] A. Bensaoula,[116] S. Beole,[24] Y. Berdnikov,[140] A. Berdnikova,[94] L. Bergmann,[94] M. G. Besoiu,[63] L. Betev,[32] P. P. Bhaduri,[135] A. Bhasin,[91] B. Bhattacharjee,[41] L. Bianchi,[24] J. Bielčík,[34] J. Bielčíková,[86] A. P. Bigot,[129] A. Bilandzic,[95] G. Biro,[46] S. Biswas,[4] N. Bize,[103] J. T. Blair,[108] D. Blau,[140] M. B. Blidaru,[97] N. Bluhme,[38] C. Blume,[64] G. Boca,[21,55] F. Bock,[87] T. Bodova,[20] J. Bok,[16] L. Boldizsár,[46] M. Bombara,[36] P. M. Bond,[32] G. Bonomi,[55,134] H. Borel,[130] A. Borissov,[140] A. G. Borquez Carcamo,[94] E. Botta,[24] Y. E. M. Bouziani,[64] L. Bratrud,[64] P. Braun-Munzinger,[97] M. Bregant,[110] M. Broz,[34] G. E. Bruno,[31,96] V. D. Buchakchiev,[35] M. D. Buckland,[85] D. Budnikov,[140] H. Buesching,[64] S. Bufalino,[29] P. Buhler,[102] N. Burmasov,[140] Z. Buthelezi,[68,123] A. Bylinkin,[20] S. A. Bysiak,[107] J. C. Cabanillas Noris,[109] M. F. T. Cabrera,[116] M. Cai,[6] H. Caines,[138] A. Caliva,[28] E. Calvo Villar,[101] J. M. M. Camacho,[109] P. Camerini,[23] F. D. M. Canedo,[110] S. L. Cantway,[138] M. Carabas,[113] A. A. Carballo,[32] F. Carnesecchi,[32] R. Caron,[128] L. A. D. Carvalho,[110] J. Castillo Castellanos,[130] M. Castoldi,[32] F. Catalano,[32] S. Cattaruzzi,[23] R. Cerri,[24] I. Chakaberia,[74] P. Chakraborty,[136] S. Chandra,[135] S. Chapeland,[32] M. Chartier,[119] S. Chattopadhay,[135] S. Chattopadhyay,[135] S. Chattopadhyay,[99] M. Chen,[39] T. Cheng,[6] C. Cheshkov,[128] V. Chibante Barroso,[32] D. D. Chinellato,[102] E. S. Chizzali,[95,b] J. Cho,[58] S. Cho,[58] P. Chochula,[32] Z. A. Chochulska,[136] D. Choudhury,[41] P. Christakoglou,[84] C. H. Christensen,[83] P. Christiansen,[75] T. Chujo,[125] M. Ciacco,[29] C. Cicalo,[52] M. R. Ciupek,[97] G. Clai,[51,c] F. Colamaria,[50] J. S. Colburn,[100] D. Colella,[31] A. Colelli,[31] M. Colocci,[25] M. Concas,[32] G. Conesa Balbastre,[73] Z. Conesa del Valle,[131] G. Contin,[23] J. G. Contreras,[34] M. L. Coquet,[103] P. Cortese,[56,133] M. R. Cosentino,[112] F. Costa,[32] S. Costanza,[21,55] C. Cot,[131] P. Crochet,[127] L. Cunqueiro,[87] M. M. Czarnynoga,[136] A. Dainese,[54] G. Dange,[38] M. C. Danisch,[94] A. Danu,[63] P. Das,[80] S. Das,[4] A. R. Dash,[126] S. Dash,[47] A. De Caro,[28] G. de Cataldo,[50] J. de Cuveland,[38] A. De Falco,[22] D. De Gruttola,[28] N. De Marco,[56] C. De Martin,[23] S. De Pasquale,[28] R. Deb,[134] R. Del Grande,[95] L. Dello Stritto,[32] W. Deng,[6] K. C. Devereaux,[18] P. Dhankher,[18] D. Di Bari,[31] A. Di Mauro,[32] B. Di Ruzza,[132] B. Diab,[130] R. A. Diaz,[7,141] T. Dietel,[114] Y. Ding,[6] J. Ditzel,[64] R. Divià,[32] Ø. Djuvsland,[20] U. Dmitrieva,[140] A. Dobrin,[63] B. Dönigus,[64] J. M. Dubinski,[136] A. Dubla,[97] P. Dupieux,[127] N. Dzalaiova,[13] T. M. Eder,[126] R. J. Ehlers,[74] F. Eisenhut,[64] R. Ejima,[92] D. Elia,[50] B. Erazmus,[103] F. Ercolessi,[25] B. Espagnon,[131] G. Eulisse,[32] D. Evans,[100] S. Evdokimov,[140] L. Fabbietti,[95] M. Faggin,[23] J. Faivre,[73] F. Fan,[6] W. Fan,[74] A. Fantoni,[49] M. Fasel,[87] A. Feliciello,[56] G. Feofilov,[140] A. Fernández Téllez,[44] L. Ferrandi,[110] M. B. Ferrer,[32] A. Ferrero,[130] C. Ferrero,[56,d] A. Ferretti,[24] V. J. G. Feuillard,[94] V. Filova,[34]

D. Finogeev,[140] F. M. Fionda,[52] E. Flatland,[32] F. Flor,[116,138] A. N. Flores,[108] S. Foertsch,[68] I. Fokin,[94] S. Fokin,[140] U. Follo,[56,d] E. Fragiacomo,[57] E. Frajna,[46] U. Fuchs,[32] N. Funicello,[28] C. Furget,[73] A. Furs,[140] T. Fusayasu,[98] J. J. Gaardhøje,[83] M. Gagliardi,[24] A. M. Gago,[101] T. Gahlaut,[47] C. D. Galvan,[109] S. Gami,[80] D. R. Gangadharan,[116] P. Ganoti,[78] C. Garabatos,[97] J. M. Garcia,[44] T. García Chávez,[44] E. Garcia-Solis,[9] C. Gargiulo,[32] P. Gasik,[97] H. M. Gaur,[38] A. Gautam,[118] M. B. Gay Ducati,[66] M. Germain,[103] R. A. Gernhaeuser,[95] C. Ghosh,[135] M. Giacalone,[51] G. Gioachin,[29] S. K. Giri,[135] P. Giubellino,[56,97] P. Giubilato,[27] A. M. C. Glaenzer,[130] P. Glässel,[94] E. Glimos,[122] D. J. Q. Goh,[76] V. Gonzalez,[137] P. Gordeev,[140] M. Gorgon,[2] K. Goswami,[48] S. Gotovac,[33] V. Grabski,[67] L. K. Graczykowski,[136] E. Grecka,[86] A. Grelli,[59] C. Grigoras,[32] V. Grigoriev,[140] S. Grigoryan,[1,141] F. Grosa,[32] J. F. Grosse-Oetringhaus,[32] R. Grosso,[97] D. Grund,[34] N. A. Grunwald,[94] G. G. Guardiano,[111] R. Guernane,[73] M. Guilbaud,[103] K. Gulbrandsen,[83] J. J. W. K. Gumprecht,[102] T. Gündem,[64] T. Gunji,[124] W. Guo,[6] A. Gupta,[91] R. Gupta,[91] R. Gupta,[48] K. Gwizdziel,[136] L. Gyulai,[46] C. Hadjidakis,[131] F. U. Haider,[91] S. Haidlova,[34] M. Haldar,[4] H. Hamagaki,[76] Y. Han,[139] B. G. Hanley,[137] R. Hannigan,[108] J. Hansen,[75] M. R. Haque,[97] J. W. Harris,[138] A. Harton,[9] M. V. Hartung,[64] H. Hassan,[117] D. Hatzifotiadou,[51] P. Hauer,[42] L. B. Havener,[138] E. Hellbär,[32] H. Helstrup,[37] M. Hemmer,[64] T. Herman,[34] S. G. Hernandez,[116] G. Herrera Corral,[8] S. Herrmann,[128] K. F. Hetland,[37] B. Heybeck,[64] H. Hillemanns,[32] B. Hippolyte,[129] I. P. M. Hobus,[84] F. W. Hoffmann,[70] B. Hofman,[59] G. H. Hong,[139] M. Horst,[95] A. Horzyk,[2] Y. Hou,[6] P. Hristov,[32] P. Huhn,[64] L. M. Huhta,[117] T. J. Humanic,[88] A. Hutson,[116] D. Hutter,[38] M. C. Hwang,[18] R. Ilkaev,[140] M. Inaba,[125] G. M. Innocenti,[32] M. Ippolitov,[140] A. Isakov,[84] T. Isidori,[118] M. S. Islam,[99] S. Iurchenko,[140] M. Ivanov,[97] M. Ivanov,[13] V. Ivanov,[140] K. E. Iversen,[75] M. Jablonski,[2] B. Jacak,[18,74] N. Jacazio,[25] P. M. Jacobs,[74] S. Jadlovska,[106] J. Jadlovsky,[106] S. Jaelani,[82] C. Jahnke,[110] M. J. Jakubowska,[136] M. A. Janik,[136] T. Janson,[70] S. Ji,[16] S. Jia,[10] T. Jiang,[10] A. A. P. Jimenez,[65] F. Jonas,[74] D. M. Jones,[119] J. M. Jowett,[32,97] J. Jung,[64] M. Jung,[64] A. Junique,[32] A. Jusko,[100] J. Kaewjai,[105] P. Kalinak,[60] A. Kalweit,[32] A. Karasu Uysal,[72] D. Karatovic,[89] N. Karatzenis,[100] O. Karavichev,[140] T. Karavicheva,[140] E. Karpechev,[140] M. J. Karwowska,[32,136] U. Kebschull,[70] M. Keil,[32] B. Ketzer,[42] J. Keul,[64] S. S. Khade,[48] A. M. Khan,[120] S. Khan,[15] A. Khanzadeev,[140] Y. Kharlov,[140] A. Khatun,[118] A. Khuntia,[34] Z. Khuranova,[64] B. Kileng,[37] B. Kim,[104] C. Kim,[16] D. J. Kim,[117] E. J. Kim,[69] J. Kim,[139] J. Kim,[58] J. Kim,[32,69] M. Kim,[18] S. Kim,[17] T. Kim,[139] K. Kimura,[92] A. Kirkova,[35] S. Kirsch,[64] I. Kisel,[38] S. Kiselev,[140] A. Kisiel,[136] J. P. Kitowski,[2] J. L. Klay,[5] J. Klein,[32] S. Klein,[74] C. Klein-Bösing,[126] M. Kleiner,[64] T. Klemenz,[95] A. Kluge,[32] C. Kobdaj,[105] R. Kohara,[124] T. Kollegger,[97] A. Kondratyev,[141] N. Kondratyeva,[140] J. Konig,[64] S. A. Konigstorfer,[95] P. J. Konopka,[32] G. Kornakov,[136] M. Korwieser,[95] S. D. Koryciak,[2] C. Koster,[84] A. Kotliarov,[86] N. Kovacic,[89] V. Kovalenko,[140] M. Kowalski,[107] V. Kozhuharov,[35] G. Kozlov,[38] I. Králik,[60] A. Kravčáková,[36] L. Krcal,[32,38] M. Krivda,[60,100] F. Krizek,[86] K. Krizkova Gajdosova,[32] C. Krug,[66] M. Krüger,[64] D. M. Krupova,[34] E. Kryshen,[140] V. Kučera,[58] C. Kuhn,[129] P. G. Kuijer,[84] T. Kumaoka,[125] D. Kumar,[135] L. Kumar,[90] N. Kumar,[90] S. Kumar,[50] S. Kundu,[32] P. Kurashvili,[79] A. B. Kurepin,[140] A. Kuryakin,[140] S. Kushpil,[86] V. Kuskov,[140] M. Kutyla,[136] A. Kuznetsov,[141] M. J. Kweon,[58] Y. Kwon,[139] S. L. La Pointe,[38] P. La Rocca,[26] A. Lakrathok,[105] M. Lamanna,[32] A. R. Landou,[73] R. Langoy,[121] P. Larionov,[32] E. Laudi,[32] L. Lautner,[32,95] R. A. N. Laveaga,[109] R. Lavicka,[102] R. Lea,[55,134] H. Lee,[104] I. Legrand,[45] G. Legras,[126] J. Lehrbach,[38] A. M. Lejeune,[34] T. M. Lelek,[2] R. C. Lemmon,[85,a] I. León Monzón,[109] M. M. Lesch,[95] E. D. Lesser,[18] P. Lévai,[46] M. Li,[6] P. Li,[10] X. Li,[10] B. E. Liang-Gilman,[18] J. Lien,[121] R. Lietava,[100] I. Likmeta,[116] B. Lim,[24] S. H. Lim,[16] V. Lindenstruth,[38] C. Lippmann,[97] D. H. Liu,[6] J. Liu,[119] G. S. S. Liveraro,[111] I. M. Lofnes,[20] C. Loizides,[87] S. Lokos,[107] J. Lömker,[59] X. Lopez,[127] E. López Torres,[7] C. Lotteau,[128] P. Lu,[97,120] Z. Lu,[10] F. V. Lugo,[67] J. R. Luhder,[126] M. Lunardon,[27] G. Luparello,[57] Y. G. Ma,[39] M. Mager,[32] A. Maire,[129] E. M. Majerz,[2] M. V. Makariev,[35] M. Malaev,[140] G. Malfattore,[25] N. M. Malik,[91] S. K. Malik,[91] L. Malinina,[141,a,e] D. Mallick,[131] N. Mallick,[48] G. Mandaglio,[30,53] S. K. Mandal,[79] A. Manea,[63] V. Manko,[140] F. Manso,[127] V. Manzari,[50] Y. Mao,[6] R. W. Marcjan,[2] G. V. Margagliotti,[23] A. Margotti,[51] A. Marín,[97] C. Markert,[108] C. F. B. Marquez,[31] P. Martinengo,[32] M. I. Martínez,[44] G. Martínez García,[103] M. P. P. Martins,[110] S. Masciocchi,[97] M. Masera,[24] A. Masoni,[52] L. Massacrier,[131] O. Massen,[59] A. Mastroserio,[50,132] O. Matonoha,[75] S. Mattiazzo,[27] A. Matyja,[107] F. Mazzaschi,[24,32] M. Mazzilli,[116] Y. Melikyan,[43] M. Melo,[110] A. Menchaca-Rocha,[67] J. E. M. Mendez,[65] E. Meninno,[102] A. S. Menon,[116] M. W. Menzel,[32,94] M. Meres,[13] Y. Miake,[125] L. Micheletti,[32] D. Mihai,[113] D. L. Mihaylov,[95] K. Mikhaylov,[140,141]

N. Minafra,[118] D. Miśkowiec,[97] A. Modak,[134] B. Mohanty,[80] M. Mohisin Khan,[15,f] M. A. Molander,[43] S. Monira,[136] C. Mordasini,[117] D. A. Moreira De Godoy,[126] I. Morozov,[140] A. Morsch,[32] T. Mrnjavac,[32] V. Muccifora,[49] S. Muhuri,[135] J. D. Mulligan,[74] A. Mulliri,[22] M. G. Munhoz,[110] R. H. Munzer,[64] H. Murakami,[124] S. Murray,[114] L. Musa,[32] J. Musinsky,[60] J. W. Myrcha,[136] B. Naik,[123] A. I. Nambrath,[18] B. K. Nandi,[47] R. Nania,[51] E. Nappi,[50] A. F. Nassirpour,[17] V. Nastase,[113] A. Nath,[94] S. Nath,[135] C. Nattrass,[122] M. N. Naydenov,[35] A. Neagu,[19] A. Negru,[113] E. Nekrasova,[140] L. Nellen,[65] R. Nepeivoda,[75] S. Nese,[19] N. Nicassio,[31] B. S. Nielsen,[83] E. G. Nielsen,[83] S. Nikolaev,[140] S. Nikulin,[140] V. Nikulin,[140] F. Noferini,[51] S. Noh,[12] P. Nomokonov,[141] J. Norman,[119] N. Novitzky,[87] P. Nowakowski,[136] A. Nyanin,[140] J. Nystrand,[20] S. Oh,[17] A. Ohlson,[75] V. A. Okorokov,[140] J. Oleniacz,[136] A. Onnerstad,[117] C. Oppedisano,[56] A. Ortiz Velasquez,[65] J. Otwinowski,[107] M. Oya,[92] K. Oyama,[76] Y. Pachmayer,[94] S. Padhan,[47] D. Pagano,[55,134] G. Paić,[65] S. Paisano-Guzmán,[44] A. Palasciano,[50] I. Panasenko,[75] S. Panebianco,[130] C. Pantouvakis,[27] H. Park,[125] H. Park,[104] J. Park,[125] J. E. Parkkila,[32] Y. Patley,[47] R. N. Patra,[50] B. Paul,[135] H. Pei,[6] T. Peitzmann,[59] X. Peng,[11] M. Pennisi,[24] S. Perciballi,[24] D. Peresunko,[140] G. M. Perez,[7] Y. Pestov,[140] M. T. Petersen,[83] V. Petrov,[140] M. Petrovici,[45] S. Piano,[57] M. Pikna,[13] P. Pillot,[103] O. Pinazza,[32,51] L. Pinsky,[116] C. Pinto,[95] S. Pisano,[49] M. Płoskoń,[74] M. Planinic,[89] F. Pliquett,[64] D. K. Plociennik,[2] M. G. Poghosyan,[87] B. Polichtchouk,[140] S. Politano,[29] N. Poljak,[89] A. Pop,[45] S. Porteboeuf-Houssais,[127] V. Pozdniakov,[141,a] I. Y. Pozos,[44] K. K. Pradhan,[48] S. K. Prasad,[4] S. Prasad,[48] R. Preghenella,[51] F. Prino,[56] C. A. Pruneau,[137] I. Pshenichnov,[140] M. Puccio,[32] S. Pucillo,[24] S. Qiu,[84] L. Quaglia,[24] A. M. K. Radhakrishnan,[48] S. Ragoni,[14] A. Rai,[138] A. Rakotozafindrabe,[130] L. Ramello,[56,133] F. Rami,[129] M. Rasa,[26] S. S. Räsänen,[43] R. Rath,[51] M. P. Rauch,[20] I. Ravasenga,[32] K. F. Read,[87,122] C. Reckziegel,[112] A. R. Redelbach,[38] K. Redlich,[79,g] C. A. Reetz,[97] H. D. Regules-Medel,[44] A. Rehman,[20] F. Reidt,[32] H. A. Reme-Ness,[37] K. Reygers,[94] A. Riabov,[140] V. Riabov,[140] R. Ricci,[28] M. Richter,[20] A. A. Riedel,[95] W. Riegler,[32] A. G. Riffero,[24] M. Rignanese,[27] C. Ripoli,[28] C. Ristea,[63] M. V. Rodriguez,[32] M. Rodríguez Cahuantzi,[44] S. A. Rodríguez Ramírez,[44] K. Røed,[19] R. Rogalev,[140] E. Rogochaya,[141] T. S. Rogoschinski,[64] D. Rohr,[32] D. Röhrich,[20] S. Rojas Torres,[34] P. S. Rokita,[136] G. Romanenko,[25] F. Ronchetti,[32] E. D. Rosas,[65] K. Roslon,[136] A. Rossi,[54] A. Roy,[48] S. Roy,[47] N. Rubini,[25,51] J. A. Rudolph,[84] D. Ruggiano,[136] R. Rui,[23] P. G. Russek,[2] R. Russo,[84] A. Rustamov,[81] E. Ryabinkin,[140] Y. Ryabov,[140] A. Rybicki,[107] J. Ryu,[16] W. Rzesa,[136] B. Sabiu,[51] S. Sadovsky,[140] J. Saetre,[20] K. Šafařík,[34,a] S. Saha,[80] B. Sahoo,[48] R. Sahoo,[48] S. Sahoo,[61] D. Sahu,[48] P. K. Sahu,[61] J. Saini,[135] K. Sajdakova,[36] S. Sakai,[125] M. P. Salvan,[97] S. Sambyal,[91] D. Samitz,[102] I. Sanna,[32,95] T. B. Saramela,[110] D. Sarkar,[83] P. Sarma,[41] V. Sarritzu,[22] V. M. Sarti,[95] M. H. P. Sas,[32] S. Sawan,[80] E. Scapparone,[51] J. Schambach,[87] H. S. Scheid,[64] C. Schiaua,[45] R. Schicker,[94] F. Schlepper,[94] A. Schmah,[97] C. Schmidt,[97] H. R. Schmidt,[93] M. O. Schmidt,[32] M. Schmidt,[93] N. V. Schmidt,[87] A. R. Schmier,[122] R. Schotter,[102,129] A. Schröter,[38] J. Schukraft,[32] K. Schweda,[97] G. Scioli,[25] E. Scomparin,[56] J. E. Seger,[14] Y. Sekiguchi,[124] D. Sekihata,[124] M. Selina,[84] I. Selyuzhenkov,[97] S. Senyukov,[129] J. J. Seo,[94] D. Serebryakov,[140] L. Serkin,[65,h] L. Šerkšnytė,[95] A. Sevcenco,[63] T. J. Shaba,[68] A. Shabetai,[103] R. Shahoyan,[32] A. Shangaraev,[140] B. Sharma,[91] D. Sharma,[47] H. Sharma,[54] M. Sharma,[91] S. Sharma,[76] S. Sharma,[91] U. Sharma,[91] A. Shatat,[131] O. Sheibani,[116] K. Shigaki,[92] M. Shimomura,[77] J. Shin,[12] S. Shirinkin,[140] Q. Shou,[39] Y. Sibiriak,[140] S. Siddhanta,[52] T. Siemiarczuk,[79] T. F. Silva,[110] D. Silvermyr,[75] T. Simantathammakul,[105] R. Simeonov,[35] B. Singh,[91] B. Singh,[95] K. Singh,[48] R. Singh,[80] R. Singh,[91] R. Singh,[97] S. Singh,[15] V. K. Singh,[135] V. Singhal,[135] T. Sinha,[99] B. Sitar,[13] M. Sitta,[56,133] T. B. Skaali,[19] G. Skorodumovs,[94] N. Smirnov,[138] R. J. M. Snellings,[59] E. H. Solheim,[19] J. Song,[16] C. Sonnabend,[32,97] J. M. Sonneveld,[84] F. Soramel,[27] A. B. Soto-Hernandez,[88] R. Spijkers,[84] I. Sputowska,[107] J. Staa,[75] J. Stachel,[94] I. Stan,[63] P. J. Steffanic,[122] T. Stellhorn,[126] S. F. Stiefelmaier,[94] D. Stocco,[103] I. Storehaug,[19] N. J. Strangmann,[64] P. Stratmann,[126] S. Strazzi,[25] A. Sturniolo,[30,53] C. P. Stylianidis,[84] A. A. P. Suaide,[110] C. Suire,[131] M. Sukhanov,[140] M. Suljic,[32] R. Sultanov,[140] V. Sumberia,[91] S. Sumowidagdo,[82] M. Szymkowski,[136] L. H. Tabares,[7] S. F. Taghavi,[95] G. Taillepied,[97] J. Takahashi,[111] G. J. Tambave,[80] S. Tang,[6] Z. Tang,[120] J. D. Tapia Takaki,[118] N. Tapus,[113] L. A. Tarasovicova,[36] M. G. Tarzila,[45] G. F. Tassielli,[31] A. Tauro,[32] A. Tavira García,[131] G. Tejeda Muñoz,[44] L. Terlizzi,[24] C. Terrevoli,[50] S. Thakur,[4] D. Thomas,[108] A. Tikhonov,[140] N. Tiltmann,[32,126] A. R. Timmins,[116] M. Tkacik,[106] T. Tkacik,[106] A. Toia,[64] R. Tokumoto,[92] S. Tomassini,[25] K. Tomohiro,[92] N. Topilskaya,[140] M. Toppi,[49] V. V. Torres,[103] A. G. Torres Ramos,[31] A. Trifiró,[30,53] T. Triloki,[96]

A. S. Triolo,[30,32,53] S. Tripathy,[32] T. Tripathy,[47] S. Trogolo,[24] V. Trubnikov,[3] W. H. Trzaska,[117] T. P. Trzcinski,[136] C. Tsolanta,[19] R. Tu,[39] A. Tumkin,[140] R. Turrisi,[54] T. S. Tveter,[19] K. Ullaland,[20] B. Ulukutlu,[95] S. Upadhyaya,[107] A. Uras,[128] M. Urioni,[134] G. L. Usai,[22] M. Vala,[36] N. Valle,[55] L. V. R. van Doremalen,[59] M. van Leeuwen,[84] C. A. van Veen,[94] R. J. G. van Weelden,[84] P. Vande Vyvre,[32] D. Varga,[46] Z. Varga,[46] P. Vargas Torres,[65] M. Vasileiou,[78] A. Vasiliev,[140,a] O. Vázquez Doce,[49] O. Vazquez Rueda,[116] V. Vechernin,[140] E. Vercellin,[24] S. Vergara Limón,[44] R. Verma,[47] L. Vermunt,[97] R. Vértesi,[46] M. Verweij,[59] L. Vickovic,[33] Z. Vilakazi,[123] O. Villalobos Baillie,[100] A. Villani,[23] A. Vinogradov,[140] T. Virgili,[28] M. M. O. Virta,[117] A. Vodopyanov,[141] B. Volkel,[32] M. A. Völkl,[94] S. A. Voloshin,[137] G. Volpe,[31] B. von Haller,[32] I. Vorobyev,[32] N. Vozniuk,[140] J. Vrláková,[36] J. Wan,[39] C. Wang,[39] D. Wang,[39] Y. Wang,[39] Y. Wang,[6] Z. Wang,[39] A. Wegrzynek,[32] F. T. Weiglhofer,[38] S. C. Wenzel,[32] J. P. Wessels,[126] J. Wiechula,[64] J. Wikne,[19] G. Wilk,[79] J. Wilkinson,[97] G. A. Willems,[126] B. Windelband,[94] M. Winn,[130] J. R. Wright,[108] W. Wu,[39] Y. Wu,[120] Z. Xiong,[120] R. Xu,[6] A. Yadav,[42] A. K. Yadav,[135] Y. Yamaguchi,[92] S. Yang,[20] S. Yano,[92] E. R. Yeats,[18] Z. Yin,[6] I.-K. Yoo,[16] J. H. Yoon,[58] H. Yu,[12] S. Yuan,[20] A. Yuncu,[94] V. Zaccolo,[23] C. Zampolli,[32] F. Zanone,[94] N. Zardoshti,[32] A. Zarochentsev,[140] P. Závada,[62] N. Zaviyalov,[140] M. Zhalov,[140] B. Zhang,[6,94] C. Zhang,[130] L. Zhang,[39] M. Zhang,[6,127] M. Zhang,[6] S. Zhang,[39] X. Zhang,[6] Y. Zhang,[120] Z. Zhang,[6] M. Zhao,[10] V. Zherebchevskii,[140] Y. Zhi,[10] D. Zhou,[6] Y. Zhou,[83] J. Zhu,[6,54] S. Zhu,[120] Y. Zhu,[6] S. C. Zugravel,[56] and N. Zurlo[55,134]

(ALICE Collaboration)

[1]*A.I. Alikhanyan National Science Laboratory (Yerevan Physics Institute) Foundation, Yerevan, Armenia*
[2]*AGH University of Krakow, Cracow, Poland*
[3]*Bogolyubov Institute for Theoretical Physics, National Academy of Sciences of Ukraine, Kiev, Ukraine*
[4]*Bose Institute, Department of Physics and Centre for Astroparticle Physics and Space Science (CAPSS), Kolkata, India*
[5]*California Polytechnic State University, San Luis Obispo, California, United States*
[6]*Central China Normal University, Wuhan, China*
[7]*Centro de Aplicaciones Tecnológicas y Desarrollo Nuclear (CEADEN), Havana, Cuba*
[8]*Centro de Investigación y de Estudios Avanzados (CINVESTAV), Mexico City and Merida, Mexico*
[9]*Chicago State University, Chicago, Illinois, United States*
[10]*China Institute of Atomic Energy, Beijing, China*
[11]*China University of Geosciences, Wuhan, China*
[12]*Chungbuk National University, Cheongju, Republic of Korea*
[13]*Comenius University Bratislava, Faculty of Mathematics, Physics and Informatics, Bratislava, Slovak Republic*
[14]*Creighton University, Omaha, Nebraska, United States*
[15]*Department of Physics, Aligarh Muslim University, Aligarh, India*
[16]*Department of Physics, Pusan National University, Pusan, Republic of Korea*
[17]*Department of Physics, Sejong University, Seoul, Republic of Korea*
[18]*Department of Physics, University of California, Berkeley, California, United States*
[19]*Department of Physics, University of Oslo, Oslo, Norway*
[20]*Department of Physics and Technology, University of Bergen, Bergen, Norway*
[21]*Dipartimento di Fisica, Università di Pavia, Pavia, Italy*
[22]*Dipartimento di Fisica dell'Università and Sezione INFN, Cagliari, Italy*
[23]*Dipartimento di Fisica dell'Università and Sezione INFN, Trieste, Italy*
[24]*Dipartimento di Fisica dell'Università and Sezione INFN, Turin, Italy*
[25]*Dipartimento di Fisica e Astronomia dell'Università and Sezione INFN, Bologna, Italy*
[26]*Dipartimento di Fisica e Astronomia dell'Università and Sezione INFN, Catania, Italy*
[27]*Dipartimento di Fisica e Astronomia dell'Università and Sezione INFN, Padova, Italy*
[28]*Dipartimento di Fisica 'E.R. Caianiello' dell'Università and Gruppo Collegato INFN, Salerno, Italy*
[29]*Dipartimento DISAT del Politecnico and Sezione INFN, Turin, Italy*
[30]*Dipartimento di Scienze MIFT, Università di Messina, Messina, Italy*
[31]*Dipartimento Interateneo di Fisica 'M. Merlin' and Sezione INFN, Bari, Italy*
[32]*European Organization for Nuclear Research (CERN), Geneva, Switzerland*
[33]*Faculty of Electrical Engineering, Mechanical Engineering and Naval Architecture, University of Split, Split, Croatia*
[34]*Faculty of Nuclear Sciences and Physical Engineering, Czech Technical University in Prague, Prague, Czech Republic*
[35]*Faculty of Physics, Sofia University, Sofia, Bulgaria*
[36]*Faculty of Science, P.J. Šafárik University, Košice, Slovak Republic*

[37]*Faculty of Technology, Environmental and Social Sciences, Bergen, Norway*
[38]*Frankfurt Institute for Advanced Studies, Johann Wolfgang Goethe-Universität Frankfurt, Frankfurt, Germany*
[39]*Fudan University, Shanghai, China*
[40]*Gangneung-Wonju National University, Gangneung, Republic of Korea*
[41]*Gauhati University, Department of Physics, Guwahati, India*
[42]*Helmholtz-Institut für Strahlen- und Kernphysik, Rheinische Friedrich-Wilhelms-Universität Bonn, Bonn, Germany*
[43]*Helsinki Institute of Physics (HIP), Helsinki, Finland*
[44]*High Energy Physics Group, Universidad Autónoma de Puebla, Puebla, Mexico*
[45]*Horia Hulubei National Institute of Physics and Nuclear Engineering, Bucharest, Romania*
[46]*HUN-REN Wigner Research Centre for Physics, Budapest, Hungary*
[47]*Indian Institute of Technology Bombay (IIT), Mumbai, India*
[48]*Indian Institute of Technology Indore, Indore, India*
[49]*INFN, Laboratori Nazionali di Frascati, Frascati, Italy*
[50]*INFN, Sezione di Bari, Bari, Italy*
[51]*INFN, Sezione di Bologna, Bologna, Italy*
[52]*INFN, Sezione di Cagliari, Cagliari, Italy*
[53]*INFN, Sezione di Catania, Catania, Italy*
[54]*INFN, Sezione di Padova, Padova, Italy*
[55]*INFN, Sezione di Pavia, Pavia, Italy*
[56]*INFN, Sezione di Torino, Turin, Italy*
[57]*INFN, Sezione di Trieste, Trieste, Italy*
[58]*Inha University, Incheon, Republic of Korea*
[59]*Institute for Gravitational and Subatomic Physics (GRASP), Utrecht University/Nikhef, Utrecht, Netherlands*
[60]*Institute of Experimental Physics, Slovak Academy of Sciences, Košice, Slovak Republic*
[61]*Institute of Physics, Homi Bhabha National Institute, Bhubaneswar, India*
[62]*Institute of Physics of the Czech Academy of Sciences, Prague, Czech Republic*
[63]*Institute of Space Science (ISS), Bucharest, Romania*
[64]*Institut für Kernphysik, Johann Wolfgang Goethe-Universität Frankfurt, Frankfurt, Germany*
[65]*Instituto de Ciencias Nucleares, Universidad Nacional Autónoma de México, Mexico City, Mexico*
[66]*Instituto de Física, Universidade Federal do Rio Grande do Sul (UFRGS), Porto Alegre, Brazil*
[67]*Instituto de Física, Universidad Nacional Autónoma de México, Mexico City, Mexico*
[68]*iThemba LABS, National Research Foundation, Somerset West, South Africa*
[69]*Jeonbuk National University, Jeonju, Republic of Korea*
[70]*Johann-Wolfgang-Goethe Universität Frankfurt Institut für Informatik, Fachbereich Informatik und Mathematik, Frankfurt, Germany*
[71]*Korea Institute of Science and Technology Information, Daejeon, Republic of Korea*
[72]*KTO Karatay University, Konya, Turkey*
[73]*Laboratoire de Physique Subatomique et de Cosmologie, Université Grenoble-Alpes, CNRS-IN2P3, Grenoble, France*
[74]*Lawrence Berkeley National Laboratory, Berkeley, California, United States*
[75]*Lund University Department of Physics, Division of Particle Physics, Lund, Sweden*
[76]*Nagasaki Institute of Applied Science, Nagasaki, Japan*
[77]*Nara Women's University (NWU), Nara, Japan*
[78]*National and Kapodistrian University of Athens, School of Science, Department of Physics, Athens, Greece*
[79]*National Centre for Nuclear Research, Warsaw, Poland*
[80]*National Institute of Science Education and Research, Homi Bhabha National Institute, Jatni, India*
[81]*National Nuclear Research Center, Baku, Azerbaijan*
[82]*National Research and Innovation Agency - BRIN, Jakarta, Indonesia*
[83]*Niels Bohr Institute, University of Copenhagen, Copenhagen, Denmark*
[84]*Nikhef, National institute for subatomic physics, Amsterdam, Netherlands*
[85]*Nuclear Physics Group, STFC Daresbury Laboratory, Daresbury, United Kingdom*
[86]*Nuclear Physics Institute of the Czech Academy of Sciences, Husinec-Řež, Czech Republic*
[87]*Oak Ridge National Laboratory, Oak Ridge, Tennessee, United States*
[88]*Ohio State University, Columbus, Ohio, United States*
[89]*Physics department, Faculty of science, University of Zagreb, Zagreb, Croatia*
[90]*Physics Department, Panjab University, Chandigarh, India*
[91]*Physics Department, University of Jammu, Jammu, India*
[92]*Physics Program and International Institute for Sustainability with Knotted Chiral Meta Matter (WPI-SKCM^2), Hiroshima University, Hiroshima, Japan*
[93]*Physikalisches Institut, Eberhard-Karls-Universität Tübingen, Tubingen, Germany*
[94]*Physikalisches Institut, Ruprecht-Karls-Universität Heidelberg, Heidelberg, Germany*
[95]*Physik Department, Technische Universität München, Munich, Germany*

[96]*Politecnico di Bari and Sezione INFN, Bari, Italy*
[97]*Research Division and ExtreMe Matter Institute EMMI, GSI Helmholtzzentrum für Schwerionenforschung GmbH, Darmstadt, Germany*
[98]*Saga University, Saga, Japan*
[99]*Saha Institute of Nuclear Physics, Homi Bhabha National Institute, Kolkata, India*
[100]*School of Physics and Astronomy, University of Birmingham, Birmingham, United Kingdom*
[101]*Sección Física, Departamento de Ciencias, Pontificia Universidad Católica del Perú, Lima, Peru*
[102]*Stefan Meyer Institut für Subatomare Physik (SMI), Vienna, Austria*
[103]*SUBATECH, IMT Atlantique, Nantes Université, CNRS-IN2P3, Nantes, France*
[104]*Sungkyunkwan University, Suwon City, Republic of Korea*
[105]*Suranaree University of Technology, Nakhon Ratchasima, Thailand*
[106]*Technical University of Košice, Košice, Slovak Republic*
[107]*The Henryk Niewodniczanski Institute of Nuclear Physics, Polish Academy of Sciences, Cracow, Poland*
[108]*The University of Texas at Austin, Austin, Texas, United States*
[109]*Universidad Autónoma de Sinaloa, Culiacán, Mexico*
[110]*Universidade de São Paulo (USP), São Paulo, Brazil*
[111]*Universidade Estadual de Campinas (UNICAMP), Campinas, Brazil*
[112]*Universidade Federal do ABC, Santo Andre, Brazil*
[113]*Universitatea Nationala de Stiinta si Tehnologie Politehnica Bucuresti, Bucharest, Romania*
[114]*University of Cape Town, Cape Town, South Africa*
[115]*University of Derby, Derby, United Kingdom*
[116]*University of Houston, Houston, Texas, United States*
[117]*University of Jyväskylä, Jyväskylä, Finland*
[118]*University of Kansas, Lawrence, Kansas, United States*
[119]*University of Liverpool, Liverpool, United Kingdom*
[120]*University of Science and Technology of China, Hefei, China*
[121]*University of South-Eastern Norway, Kongsberg, Norway*
[122]*University of Tennessee, Knoxville, Tennessee, United States*
[123]*University of the Witwatersrand, Johannesburg, South Africa*
[124]*University of Tokyo, Tokyo, Japan*
[125]*University of Tsukuba, Tsukuba, Japan*
[126]*Universität Münster, Institut für Kernphysik, Münster, Germany*
[127]*Université Clermont Auvergne, CNRS/IN2P3, LPC, Clermont-Ferrand, France*
[128]*Université de Lyon, CNRS/IN2P3, Institut de Physique des 2 Infinis de Lyon, Lyon, France*
[129]*Université de Strasbourg, CNRS, IPHC UMR 7178, F-67000 Strasbourg, France, Strasbourg, France*
[130]*Université Paris-Saclay, Centre d'Etudes de Saclay (CEA), IRFU, Départment de Physique Nucléaire (DPhN), Saclay, France*
[131]*Université Paris-Saclay, CNRS/IN2P3, IJCLab, Orsay, France*
[132]*Università degli Studi di Foggia, Foggia, Italy*
[133]*Università del Piemonte Orientale, Vercelli, Italy*
[134]*Università di Brescia, Brescia, Italy*
[135]*Variable Energy Cyclotron Centre, Homi Bhabha National Institute, Kolkata, India*
[136]*Warsaw University of Technology, Warsaw, Poland*
[137]*Wayne State University, Detroit, Michigan, United States*
[138]*Yale University, New Haven, Connecticut, United States*
[139]*Yonsei University, Seoul, Republic of Korea*
[140]*Affiliated with an institute covered by a cooperation agreement with CERN*
[141]*Affiliated with an international laboratory covered by a cooperation agreement with CERN*

[a]Deceased.
[b]Also at Max-Planck-Institut fur Physik, Munich, Germany.
[c]Also at Italian National Agency for New Technologies, Energy and Sustainable Economic Development (ENEA), Bologna, Italy.
[d]Also at Dipartimento DET del Politecnico di Torino, Turin, Italy.
[e]Also at An institution covered by a cooperation agreement with CERN.
[f]Also at Department of Applied Physics, Aligarh Muslim University, Aligarh, India.
[g]Also at Institute of Theoretical Physics, University of Wroclaw, Poland.
[h]Also at Facultad de Ciencias, Universidad Nacional Autónoma de México, Mexico City, Mexico.